Report No.
UCB/SEMM-2013/08

Structural Engineering
Mechanics and Materials

NONLINEAR SEISMIC SITE RESPONSE AND SOIL FOUNDATION STRUCTURE INTERACTION OF A 20-STORY STRUCTURAL WALL BUILDING SUBJECTED TO PULSE-LIKE EXCITATION

By

Yuan Lu and Marios Panagiotou

November 2013

Department of Civil and Environmental Engineering
University of California, Berkeley

Nonlinear Seismic Site Response and Soil Foundation Structure Interaction of a 20-story Structural Wall Building Subjected to Pulse-like Excitation

Yuan Lu and Marios Panagiotou

Abstract

The effect of soil-foundation-structure interaction (SFSI) for a 20-story core wall building with a caisson foundation subject to single pulse motions is investigated using two-dimensional (2D) nonlinear response history analysis. Eight soil profiles are considered with depth of soil from 20 to 220 m, shear wave velocity of 200 to 400 m/s at the surface of the soil, and an elastic rock half-space below the soil layer; nonlinear site response effects on the free-field motion and structural response is discussed. Eleven single pulse motions with period of 0.5 to 5 s and peak velocity of 0.53 m/s are the vertically propagating imposed excitation, with peak velocity at the soil surface ranging from 1.0 to 1.7 m/s. To decompose the effect of SFSI on the structural response, the response of the 2D model including soil, foundation, and structure is compared to that of a model consisting of the fixed-base 20-story super-structure subjected to the free-field motion recorded at the soil surface. The nonlinear site response effects for free-field motions result in a maximum of 64% amplification at specific pulse periods for deep soils. The SFSI has a small effect (less than 15% difference compared to the structure-only model) on the peak roof acceleration. SFSI also has a small effect (less than 10% difference) on the maximum value of peak roof drift, peak base shear force and peak roof acceleration ratio over the pulse periods considered.

Introduction

It is projected that by the year 2030, 5 billion people (60% of the world population) will live in urban areas throughout the world – an increase from 30% in 1950 and 47% in 2000 (Unchs 2001). Compared to the sprawling suburban regions, which are unsustainable because of the maintenance cost of extended infrastructure for commute and loss of arable land, multi-story buildings (defined as buildings taller than 35 m) are essential for developing sustainable urban growth (Wood 2007). Unavoidably, the number and size of urban centers located near major

earthquake faults will increase accordingly. However, urban centers located near earthquake faults are vulnerable to significant seismic damage, especially in events where the fault-rupture directivity combines with nonlinear site effects. This was most clearly demonstrated in the 2011 magnitude 6.3 Christchurch, New Zealand earthquake: 36 of the 50 tallest buildings (height of 35 m or more) in the city of Christchurch (located 5 km from the fault rupture) had to be demolished following the earthquake ("List of tallest buildings in Christchurch" 2013).

Multi-story buildings commonly have several subterranean stories supported on an embedded mat foundation, forming a caisson foundation, with or without piles. Soil-foundation-structure interaction (SFSI) adds flexibility to the structural system which changes the structural response, causing an increase or decrease in the displacement and force demands depending on the seismic excitation and structural properties (Mylonakis and Gazetas 2000).

The effect of soil-foundation interaction for machine-type and seismic excitation has been studied since the 70's [see Gazetas (1991) for an overview of the research done in that era] and the literature on seismic soil-foundation interaction for shallow foundations is extensive. Two broad classifications of numerical models used for SFSI are: (1) the "direct approach" where the structure, foundation, and surrounding soil is modeled using two- or three-dimensional finite elements and structural elements with appropriate boundary conditions; and (2) the "substructure approach" where the soil surrounding the foundation is modeled using boundary finite-elements or springs based on dynamic transfer functions. The direct approach has been used for modeling SFSI, including lateral spreading, of bridge structures both 2D (e.g. Zhang et al. 2008) and 3D (Elgamal et al. 2008, Jeremić et al. 2009). For buildings, the substructure approach [such as outlined in Stewart and Tileylioglu (2007) for tall buildings] is generally preferred due to the computational simplicity; studies including Gerolymos and Gazeta (2005) have developed macro-elements to model the soil-foundation interaction for caisson foundations including interface and soil material nonlinearity.

Sites near the fault rupture of an earthquake event are strongly affected by the rupture propagation, especially when the site is in the direction of the fault rupture (forward directivity) (Somerville and Graves 1993). These near-fault ground motions contain strong acceleration, velocity, and displacement pulses, which result in significant nonlinearity in the site soil as well as large demands in the response of structures. Studies (e.g. Seed et al. 1976) have shown that soil and site conditions can impact the surface motion and the resulting spectral values, and in

cases of soft or deep soils, this may result in amplification of long period (greater than 1 s) response. Rogriguez-Marek and Bray (2006) studied the nonlinear site response subject to single-cycle sinusoidal pulse motions. In their study, they found that both the amplitude and period of the surface motions were affected by the site response; the peak velocity of the input seismic excitation was amplified or attenuated based on the input velocity amplitude and ratio between the input velocity period and the site characteristics. The effect of near-fault pulse-like ground motions on structures has been well-studied, including the case of tall buildings having a first mode period greater than or equal to 2 s (e.g. Hall et al. 1995, Calugaru and Panagiotou 2012a); however, these studies do not include the effects of SFSI.

In this report, a 20-story core wall building with a caisson foundation without piles, including the surrounding site. The models are subject to single-cycle pulse excitation with pulse period of 0.5 to 5.0 s and peak velocity at the soil surface of 1.0 to 1.7 m/s. The study focus on two main aspects of the response: (1) the nonlinear site response; and (2) the soil-foundation-structure interaction. Eight soil profiles are considered, with the depth of soil varying between 20m and 220m and shear wave velocity at the top equal to either 200 m/s or 400 m/s with linear increase with depth.

2D Finite-Element Model Description

To investigate the SFSI and nonlinear site response effects, the following models are constructed: (a) the structure-only (SO) model, which consists of the superstructure fixed at the ground-level; (b) the free-field soil (FFS) model which represents the soil domain without the structure; (c) the soil-foundation-structure (SFS) model which models the structure, foundation, and soil domain and accounts for both the effect of the nonlinear site and the SFSI effect; and (d) a free-field rock (FFR) model of a rock outcrop with no soil. The FFS, SFS, and FFR models are subjected to a single cycle acceleration pulse with dominant period varying between 0.5 and 5 s described in *Input Excitation*. To decompose the effect of SFSI, the motion recorded at the surface of the soil in the SFS model will be used as the input ground excitation for the SO model, and the response of the SO model will be compared to that of the SFS model. In addition, the SO model with ground excitation that is recorded from the FFR model will be termed SOR (structure-on-rock).

Structure

Figure 1(a) shows the 20-story tall core-wall building [Calugaru and Panagiotou (2012b)] considered in this study. The structure has 20-stories above ground (a total height of 67 m above ground level) with 3 floors below ground and a 3.5 m thick mat foundation (total depth of 13.5m below ground level). The cracked first mode period of the fixed-base building is approximately 2 s. The structure has a total seismic weight W = 154 MN above ground (7.68 MN per floor) and 109 MN below ground including the mat foundation. The compressive strength of concrete $f_c^{'}$ = 72 MPa, with a confined concrete strength of f_{cc} = 101.4 MPa occurring at strain ε_{cc} = 0.004. The steel yield strength f_y = 414 MPa with Young's modulus E_s = 200 GPa.

Above ground, the structure consists of a central core wall coupled through the floor slab to the columns in the perimeter of the building. Figure 1(c) shows the cross-sectional details of the core wall, which has a length of 9.75 m and thickness of 0.61 m and a longitudinal reinforcement ratio ρ_l = 0.8%. The core wall is designed to provide most of the lateral force resistance above ground; based on tributary area, the core wall carries 44.2% of the gravity load (and vertical mass). The axial load ratio $N / f_c^{'} A_g$ = 0.42 at the base of the wall, where N is the axial load, $f_c^{'}$ is the concrete compressive strength, and A_g is the concrete gross area. For the three basement levels, walls are used along the perimeter of the building and from the columns to the core wall in order to distribute the forces from the super-structure to the entire width of the foundation. The structure has a square floor plan on all levels and is symmetric across the two horizontal axes.

In this study, the structure above ground level (herein referred to as the super-structure) will be modeled using two-dimensional (2D) nonlinear fiber beam-column elements, as shown in Figure 1(b); only the core-wall is modeled and the effect of framing is neglected. The core wall of each floor above ground level is modeled using one beam-column element with 4 integration points. Each fiber section has one curtain of longitudinal rebar with confined concrete over the entire concrete gross area; a total of 128 concrete and 120 steel fibers are used, one layer of both concrete and steel for each of the four sides of the core wall cross-section. Figure 1(d) and (e) show the hysteretic behavior of the material models used for the concrete and steel fibers, respectively. The structure-only (SO) model consists only of the beam-column elements used to model the super-structure, and the flexibility of the foundation is neglected; Node 0 [shown in

Figure 1(b)] is fixed for all degrees of freedom (dofs), which results in a fixed-base model similar to what is commonly used in structural analysis practice. For the soil-foundation-structure (SFS) model, Node 0 is connected to the foundation as described in the section titled *Foundation and Soil-Foundation-Structure Interface*.

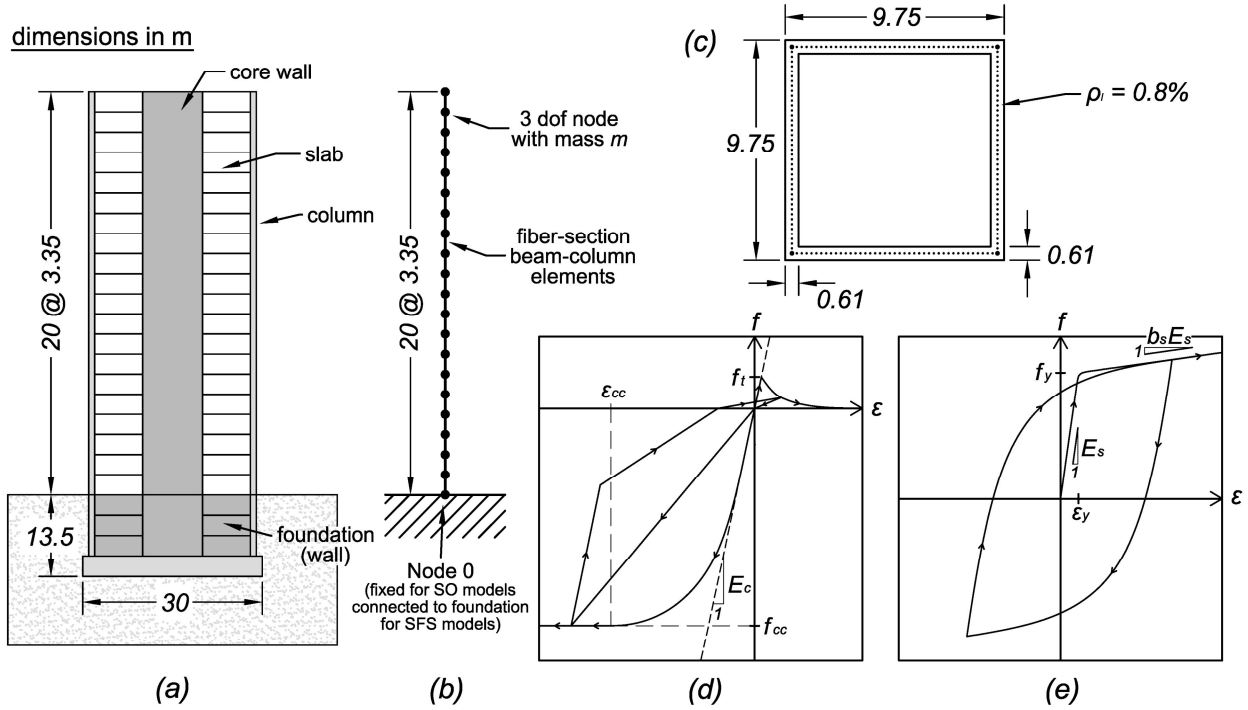

Figure 1. (a) Elevation view of the 20-story core wall building considered; (b) 2D model for superstructure; (c) cross-sectional details of the core wall; (d) concrete material stress-strain; and (e) steel material stress-strain.

Soil Domain

To model the effect of soil-foundation-structure interaction, a 2D rectangular soil domain is used in conjunction with the previously described building [shown in Figure 2(a)]. The soil is assumed to be horizontally unbounded and subject to vertically propagating shear waves from the underlying bedrock (no spatial variation along the bedrock). The validity and limitations of the imposed excitation are discussed in the section titled *Limitations.* This section describes the soil properties and boundary conditions used in this study while the next section discusses the

modeling of the foundation and the interface between the finite elements and beam-column elements.

The soil layer has a height of H_s and a width of 180 m. The soil layer until the depth of bedrock is modeled using 2D four-node nonlinear square finite elements with side length Δh. Below the soil is a linear elastic undamped half-space representing the bedrock (shear wave velocity $V_{s,rock}$ = 1200 m/s, density γ_{rock} = 23.5 kN / m^3) and is accounted for by the Lysmer-Kuhlemeyer transmitting/absorbing boundary conditions (Zhang et al. 2003) along the base of the soil layer [see Figure 2(a)]. As part of the Lysmer-Kuhlemeyer boundary, the seismic excitation is applied as a dynamic equivalent force at each node at the base of the soil domain (Zhang et al. 2003) to model the propagation of the wave from the elastic bedrock half-space; only vertically propagating shear waves are applied and details on the applied motion is presented in the section titled *Input Excitation*. The lateral boundaries of the soil domain have a "shear beam" constraint: the horizontal and vertical degrees-of-freedom (dofs) of the two vertical boundaries [line AC and BD in Figure 2(a)] are constrained to have the same motion.

The soil material used in this study is a nested Von Mises plasticity model (PressureIndependMultiYield in Opensees) with a hyperbolic backbone curve for the shear stress-strain relation, see Figure 2(a). The shear wave velocity and shear strength profile for the soil layer are assumed to be linearly increasing with depth, as shown in Figure 2(b), and the Poisson's ratio for the soil is 0.4. The shear strength at depth H is defined by:

$$S_u(H) = 0.5\gamma H \tan(\phi) + S_{u,top} \qquad \text{(Eq. 1)}$$

where the soil density γ = 20 kN / m^3, friction angle ϕ = 45º, and shear strength at the surface of the soil layer $S_{u,top}$ = 50 kPa. Eight soil profiles are considered in this study with soil layer height H_s = 20, 60, 140, and 220 m and shear wave velocity at the surface of the soil layer $V_{s,top}$ = 200 and 400 m/s are considered. Table 1 lists the soil layer height H_s, element length Δh, shear wave velocity at the surface of the soil layer $V_{s,top}$, shear wave velocity at the base of the soil layer $V_{s,bot}$, and first mode period of the soil layer T_s.

For the free-field soil (FFS) model, which models the nonlinear soil without the structure and associated SFSI effect, use a soil column model – a column of soil with depth H_s, width of 4 elements, and the same boundary conditions applied to the SFS model as described previously. A soil column model is also used for the free-field rock (FFR) model.

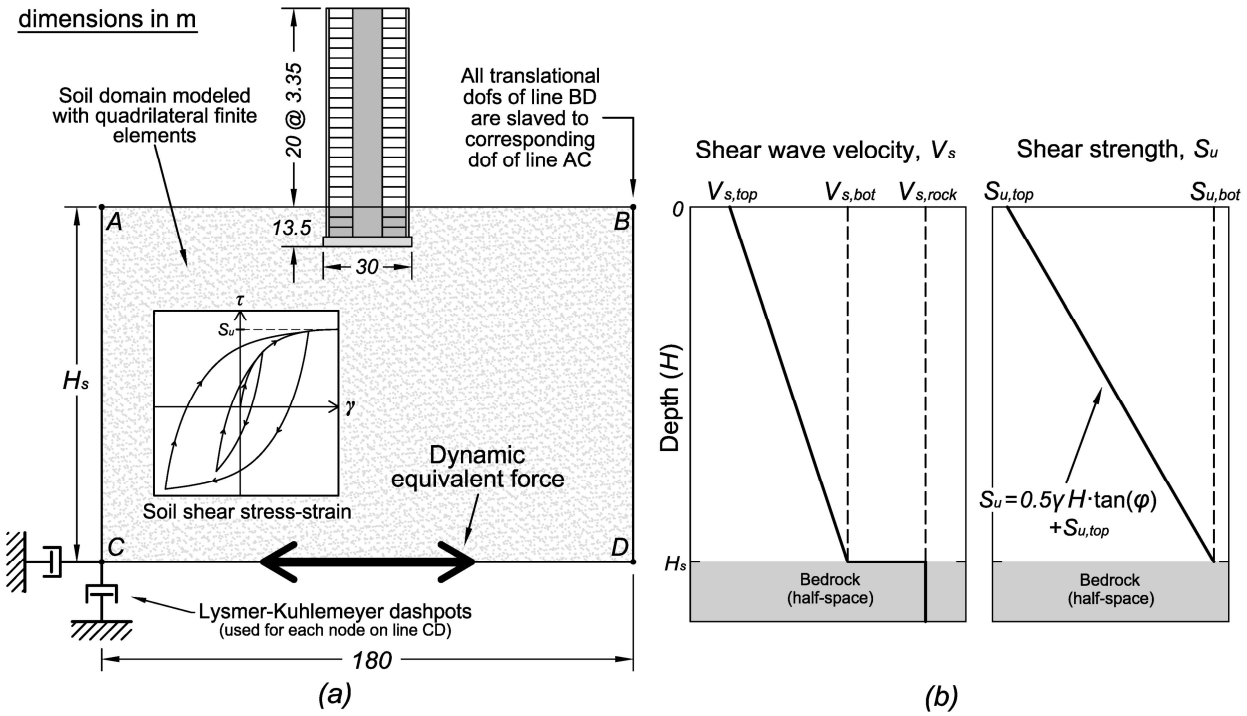

Figure 2. (a) Elevation view of the 2D soil-foundation-structure (SFS) model studied, including boundary conditions and soil shear stress-strain, and (b) shear wave velocity and shear strength profile over depth.

Table 1. Shear wave velocity V_s variation, soil layer height H_s, and initial first mode period of the soil layer T_s for the eight soil profiles considered.

Soil Profile Name	H_s (m)	Δh (m)	$V_{s,top}$ (m/s)	$V_{s,bottom}$ (m/s)	T_s (s)
H20V400	20	0.75	400	600	0.15
H20V200			200	400	0.25
H60V400	60	1.5	400	800	0.37
H60V200			200	800	0.43
H140V400	139.5	1.5	400	800	0.85
H140V200			200	800	1.0
H220V400	220.5	1.5	400	800	1.3
H220V200			200	800	1.6

Foundation and Soil-Foundation-Structure Interface

In this study, the subsurface stories and underlying mat foundation (herein collectively referred to as the foundation block) is assumed to remain elastic and are modeled using 2D linear isotropic finite elements. The total weight of the foundation block (109 MN) and corresponding mass is distributed equally across the foundation block. The elements used to model the foundation block coincide with the finite element grid used for the soil elements, allowing the adjacent soil and foundation block elements to share adjacent nodes. However, the model does not allow for uplift of the foundation from soil surface [see section *Limitations*]. The soil-foundation-structure (SFS) model consists of 2D finite elements (for the soil and foundation block; 2 dofs per node) and beam-column elements (for the super-structure; 3 dofs per node); the interface between the two types of elements is at the structure-foundation interface. At this interface, translational dofs at base of the super-structure model [translational dofs of Node 0 in Figure 1(b)] are slaved to that of the foundation block node at the same location. In order for the rotation of base of the super-structure to follow the rotation of the foundation block, Node 0 is connected to a set of rigid beams which span along the surface of the foundation.

Input Excitation

For this report, it is assumed that the soil and structure is subject to vertically propagating shear waves from the underlying bedrock, thus the ground excitation is applied only at the base of the models in the horizontal direction. The applied velocity time history is given by the waveform of Mavroeidis and Papageorgiou (2003) with oscillatory parameter $\gamma = 1$ and phase parameter $\theta = 1$:

$$v(t) = -0.5 v_P \left[1 + \cos\left(\frac{4\pi}{3T_P}(t - 0.75T_P)\right)\right] \cdot \cos\left(\frac{4\pi}{3T_P}(t - 0.75T_P)\right) \qquad 0 \le t \le \frac{3T_P}{2} \qquad \text{(Eq. 2)}$$

where v_P is the velocity amplitude and T_P is the dominant period of the pulse. Pulses with period T_P = 0.5, 0.75, 1.0, 1.5, 2.0, 2.5, 3.0, 3.5, 4.0, 4.5, and 5.0 s are considered. The amplitude of the ground excitation (for each T_P) was chosen to be about one third of the peak amplitudes of pulses

extracted from 40 historical strong near-fault ground motion records (Lu and Panagiotou 2013), and is taken to be:

$$\begin{aligned} a_p &= 0.2\, g / T_P \\ v_P &= 0.53 m / s \\ d_P &= 0.21 m \cdot T_P \end{aligned} \qquad \text{(Eq. 3)}$$

where a_p and d_P are the acceleration and displacement amplitudes, respectively. Figure 3 shows the acceleration, velocity, and displacement time history for a pulse with T_P = 1 s.

Note that the input excitation defined in this section is the wave that propagates through the bedrock – it is not necessarily equal to the motion recorded at the soil-bedrock interface (at the base of the soil layer, above the Lysmer-Kuhlemeyer boundaries) or at the top of the free-field rock (FFR) models. The Lysmer-Kuhlemeyer transmitting/absorbing boundary conditions account for the propagation of the input wave through the assumed half-space under the soil, and thus, the waves from the soil layer and the effect of the proximity of the free surface result in a different (and often stronger) motion at the top of the bedrock. In the case of the FFR models, the motion at the free-surface is twice that imposed within the bedrock due to the nature of one-dimensional wave propagation through a uniform elastic medium with a free boundary.

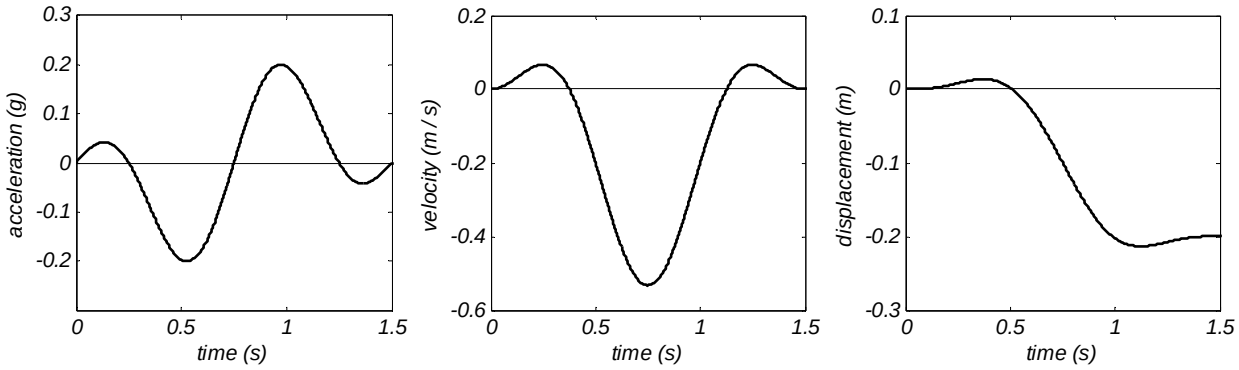

Figure 3. Acceleration, velocity, and displacement time history of a single cycle pulse with dominant pulse period T_P = 1 s and acceleration amplitude a_P = 0.2 g.

Finite-Element Analysis Program and Solution Procedure

All models were built and run in Opensees (McKenna et al. 2000). The following existing elements and material models were used: (1) for the super-structure, forced-based fiber-section

beam-column element (forceBeamColumn) with 4 Gauss-Lobatto integration points, Kent-Scott-Park concrete material with nonlinear tension softening (Concrete03), and modified Giuffré-Menegotto-Pinto steel material (Steel02); (2) for the soil, plain-strain four-node quadrilateral finite element (quad) with the Von Mises multisurface plasticity material model (PressureIndependMultiYield); (3) for the foundation block, the plain-strain quad elements with elastic isotropic material (ElasticIsotropic); and (4) for the Lysmer-Kuhlemeyer dashpots, zeroLength elements with the linear Viscous material. Rayleigh damping of 2% at periods 0.2 and 10 s is used for the soil and foundation-block nodes, and 2% damping at periods 0.8 and 3 s are used for the structure.

The analysis procedure consists of statically applied gravity loads followed by dynamic seismic excitation. The gravity is applied statically in 10 load-controlled steps. For the dynamic analysis, the Newmark time stepping algorithm ($\gamma = 0.5$, $\beta = 0.25$) is used with a time step of 0.002 s for all analysis. 20 iterations of Newton-Raphson algorithm with a tolerance of 10^{-6} is used, followed by dividing the time step by 10 and trying again. A sparse solver (UmfPack) is used to solve the system of equations at every step.

A computer with a 3.47 GHz Intel Core i7 CPU and 12GB of RAM was used for this study; a maximum of 6 hours was needed to the most computationally extensive model: the SFS models for site H220V400 and H220V200, which have a total of 35,601 dofs and 17,800 elements, analyzed for 15 seconds of dynamic analysis with time step of 0.002 s.

Nonlinear Site Response

This section presents the effect of nonlinear site response on the characteristics of the recorded free-surface response of a free-field site (no structure). This effect is investigated by comparing two models: (1) the free-field soil (FFS) models for each of the eight soil profiles, and (2) the free-field rock (FFR) model which gives the free-surface motion for an elastic rock site. The acceleration and velocity time history as well as the spectral displacement for both FFR and FFS with the eight soil profiles and eleven pulses considered is included in Appendix A.

The peak acceleration and velocity of the free-surface motion for each of the FFS and FFR models subjected to the single pulse excitation with period T_P is shown in Figures 4 and 5. As expected, the peak acceleration and velocity of the FFR models are exactly two times that of the input motion. For the FFS models, based on the assumed shear strength profile (see Eq. 1),

the maximum peak acceleration at the surface of the soil is approximately $S_{u,H_h}/(\gamma H_h)$ where $H_h = H_s/2$, the numerator is the shear strength at H_h, and the denominator is the weight of soil above H_h; this relation gives maximum peak acceleration 0.68, 0.51, 0.46, and 0.44 g for soil profiles with H_s = 20, 60, 140, and 220 m, respectively, which is within 10% error of the peak accelerations of the FFS models for T_P = 0.5 s. De-amplification of acceleration occurs for sites H20V400 and H20V200 with the T_P = 0.5 s pulse, and for the rest of the sites with $T_P \leq 0.75$ s pulses except for H220V400, where de-amplification of acceleration occurs for $T_P \leq 1.0$ s pulses. The de-amplification is partially due to the attenuation in the soil and partially due to the soil nonlinearity, including the shear strength profile which limits the maximum acceleration at the surface of the soil layer.

For the FFS models, amplification of the peak acceleration and velocity increase as the period of the soil layer increases, with FFS peak velocity ranging from 1.09 (H20V400) to 1.64 (H220V200) times that of FFR. The maximum amplification of peak acceleration occurs at T_P = 1.0, 1.5, 2.0, 2.5, and 2.5 and that of peak velocity occurs at T_P = 0.75, 1.0, 1.5, 1.5, and 2.0 for site profiles with H_s = 20, 60, and 140 m, and H220V400 and H220V200, respectively; for $V_{s,top}$ = 200 m/s models, the maximum amplification for both peak acceleration and velocity is 1.06 to 1.16 times that of models with $V_{s,top}$ = 400 m.

The peak spectral displacement Sd_{max} between T = 0.1 and 5 s for the FFR and FFS models of each soil profile is shown in Figure 6. It should be noted that the curve of Sd_{max} for the FFR model at T_P = 0.45 and 0.5 s is because of the limited oscillator period over which Sd_{max} is computed. The Sd_{max} of the FFS models are between 1.0 and 2.2 times that of the FFR models for all soil profiles considered; the range and maximum value of amplification of Sd_{max} for each soil profile increases with increasing period of the soil layer. For the first seven soil profiles in the order listed in Table 1 (H20V400, H20V200, H60V400, H60V200, H140V400, H140V200, H220V400), the Sd_{max} of the FFS model is less than 1.1 times that of the FFR model for T_P greater than or equal to 0.75, 1.0, 1.5, 1.5, 2.5, 3.0, 4.5 s, which is $T_P / T_s \geq 3.6$. For the H220V200 model, the FFS model resulted in Sd_{max} that is 1.15 times that of the FFR model at T_P = 5.0 s pulse.

Figure 7 shows T_{max}, the oscillator period at which Sd_{max} occurs, and $T[0.9Sd_{max}]$, the range of oscillator periods that result in a spectral displacement greater than or equal to 0.9 times Sd_{max}. Note, for the FFR model, the $T[0.9Sd_{max}]$ range spans from approximately $T = T_P$ to 5 s.

For the FFS models with site profiles H20V400, H20V200, H60V400, and H60V200, there is negligible change in the $T[0.9Sd_{max}]$ range, which indicates that, though some amplification of Sd occurs, the overall shape of the computed spectral displacement does not change. However, for the site profiles H140V400, H140V200, H220V400, and H220V200, the $T[0.9Sd_{max}]$ range lies between 1 and 3 s for pulses with $T_P \leq 1$ s. This is especially noticeable in the soil profile H220V200 with a $T_P = 0.5$ s pulse where $T_{max} = 1.7$ s and $T[0.9Sd_{max}] = 1.4 – 2.1$ s; in this case, the nonlinear soil domain distorts and elongates the pulse so that dominant acceleration pulse has a period of about 1.2 s, with a small amplitude cycle of period of 2.0 s due to reflection from the soil-bedrock interface. The acceleration and velocity time history as well as the spectral displacement is included in Appendix A.

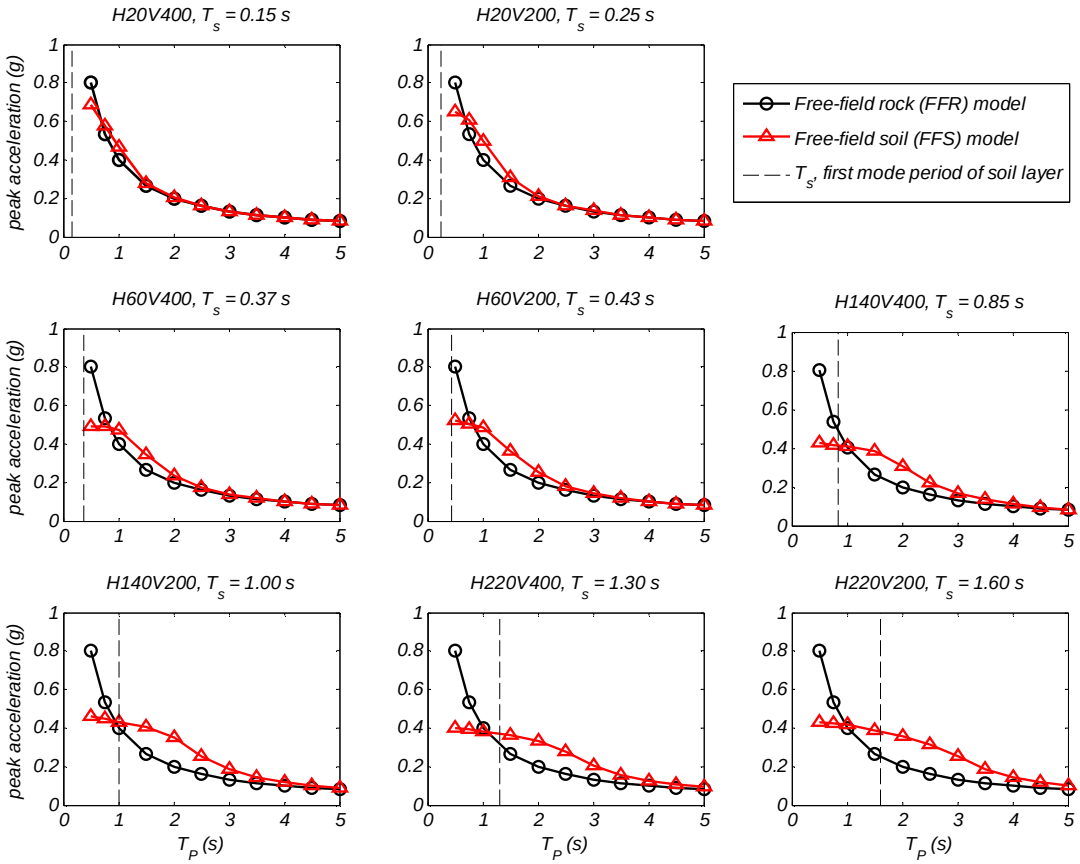

Figure 4. Peak acceleration at the free-surface of the free-field rock (FFR) model compared with that of the free-field soil (FFS) models of each of the sites subjected to a single pulse of T_P ranging from 0.5 to 5 s.

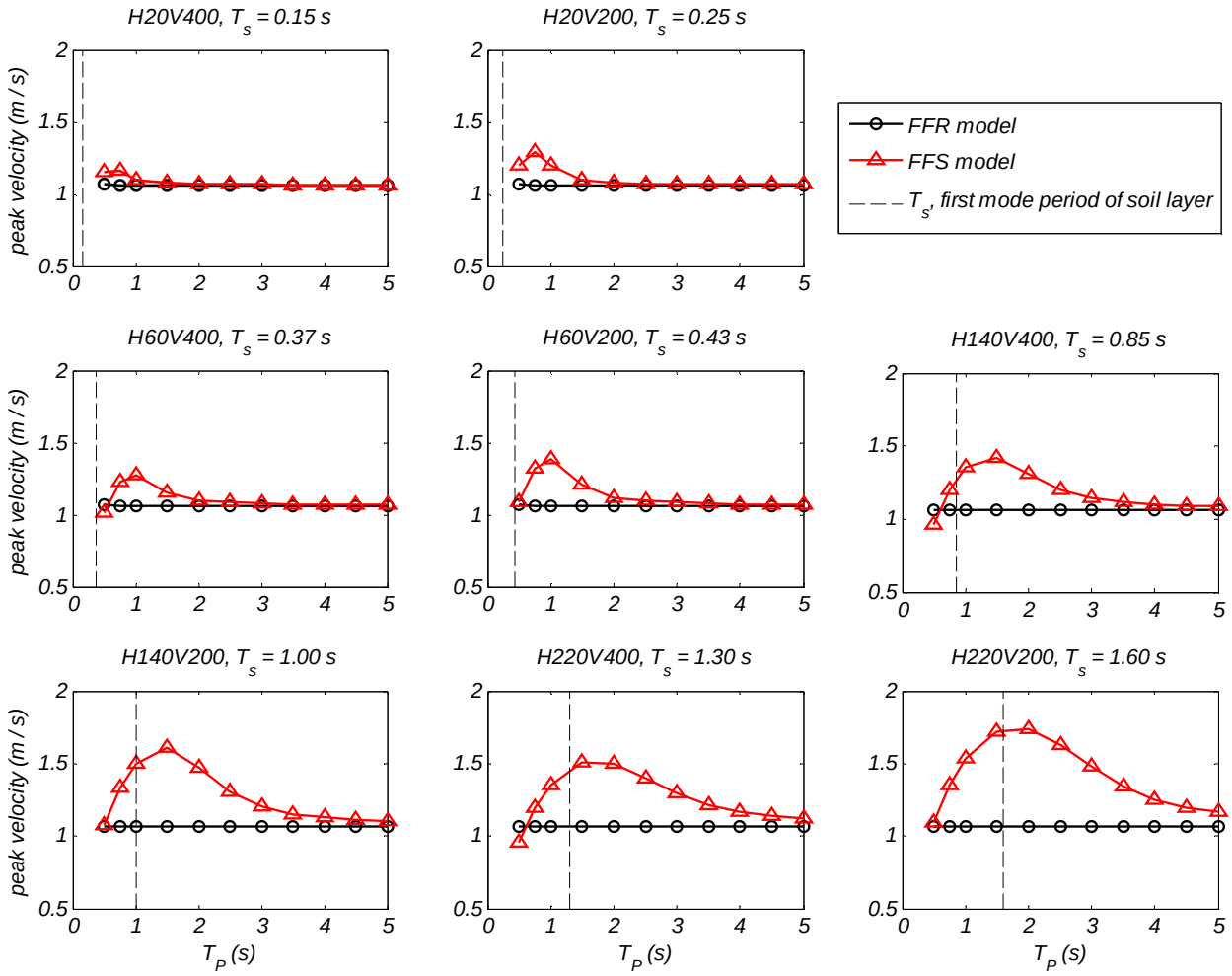

Figure 5. Peak velocity at the free-surface of the free-field rock (FFR) model compared with that of the free-field soil (FFS) models of each of the sites subjected to a single pulse of T_P ranging from 0.5 to 5 s.

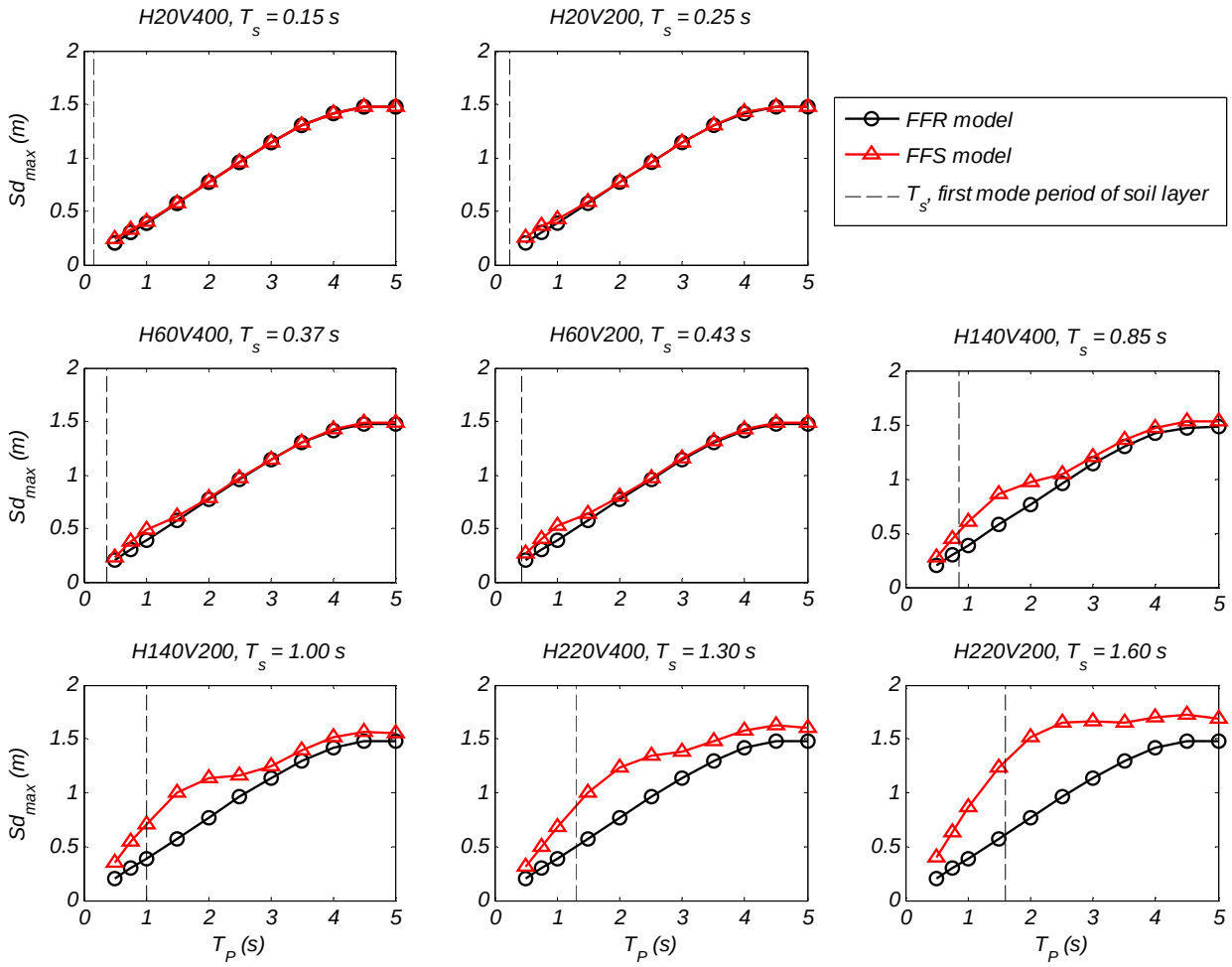

Figure 6. Peak value of spectral displacement Sd_{max} (for T between 0.1 and 5 s) for motions at the free-surface of the free-field rock (FFR) model compared with that of the free-field soil (FFS) models of each of the sites subjected to a single pulse of T_P ranging from 0.5 to 5 s.

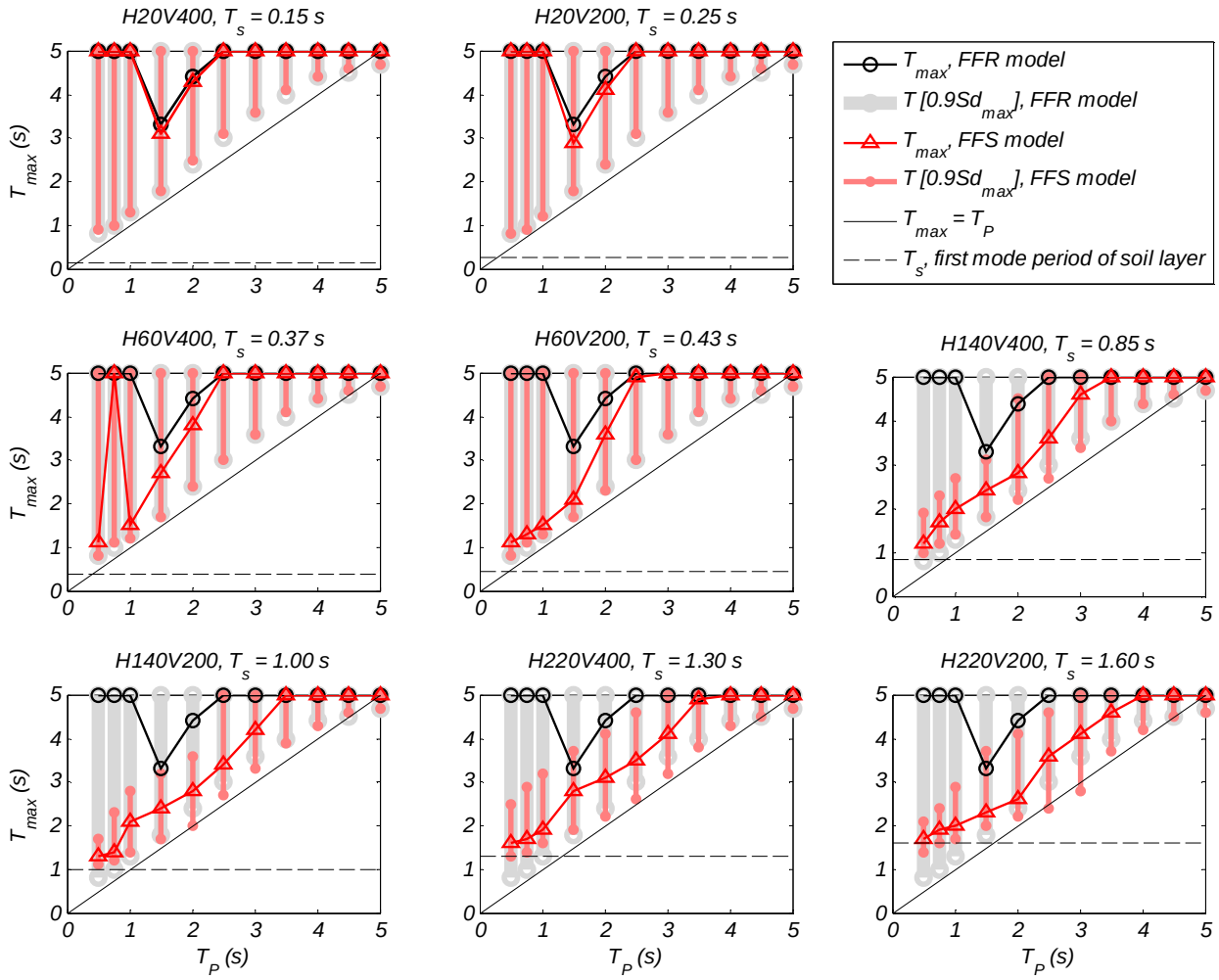

Figure 7. Maximum and minimum values of T (between 0.1 and 5 s) where spectral displacement is greater than 90% of Sd_{max} for motions at the free-surface of the free-field rock (FFR) model compared with that of the free-field soil (FFS) models of each of the sites subjected to a single pulse of T_P ranging from 0.5 to 5 s.

Dynamic Soil-Foundation-Structure Interaction

This section presents the effect of soil-foundation-structure interaction (SFSI) on the response of the 20-story structural wall building. The effect of SFSI with and without the nonlinear soil effect is investigated by comparing three models: (1) the structure-on-rock (SOR) model, which consists of the 20-story super-structure subjected to the motions recorded at the surfaces of the FFR model; (2) the structure-only (SO) model, which consists of the 20-story super-structure subjected to the motions recorded at the surfaces of the FFS models for each soil profile; and (3) the soil-foundation-structure (SFS) model which includes the soil domain, foundation block, and structure as discussed in the section titled *2D Finite-Element Model Description*.

The peak roof drift ratio Θ_r for the super-structure, peak roof acceleration a_r, and peak base shear V_b normalized by the weight of the super-structure W, are shown in Figures 8, 9, and 10, respectively. For the peak roof drift ratios shown in Figure 8, the difference between SOR and SO is as expected from the results presented in section *Nonlinear Site Response* and is consistent with the trends of peak velocity amplification shown in Figure 5. The SFS models result in a peak roof drift ratio that is similar (less than 8% difference) to that of the SO models for pulses with period $T_P \leq 2.5$ s (for H_s = 20, 60, and 140 m) and $T_P \leq 3.0$ s (for H_s = 220 m). The SO, SFS, and SOR models all results in less than 0.5% peak roof drift ratio for $T_P \geq 4.0$ s (for H_s = 20, 60, and 140 m) and $T_P \geq 4.5$ s (for H_s = 220 m), indicating an elastic response for those pulse excitations regardless of the effect of soil. For the pulses with $3.0 \leq T_P \leq 3.5$ s (for H_s = 20, 60, and 140 m) and $3.5 < T_P < 4.0$ s (for H_s = 220 m), the SFS models compute a peak roof drift ratio that is 1.3 – 2.3 times that of the SO models; however, the maximum value of peak roof drift ratio over the period range for the SFS and SO models are less than 7% different. In this region, the peak roof drift ratio of the SFS model at a pulse period of T_P gives a similar value as that of the SO model at a pulse period of (T_P – 0.25 s).

For the peak roof accelerations shown in Figure 9, the difference between SOR and SO is similar to that of peak acceleration at the surface of the soil discussed in the previous section; the peak roof acceleration of the SOR model decreases linearly for $T_P \geq 1.5$ s, compared to the nearly exponential decrease of peak acceleration at the surface of the soil (shown in Figure 4), because of the influence of the period of the super-structure (cracked first mode period of 2 s). For the soil profiles with H_s = 20 and 60 m, there is negligible difference between the SOR and

SO models for $T_P \geq 2$ s. However, for the soil profiles with H_s = 140 and 220 m, there is a local maximum of peak roof acceleration for the SO and SFS models at T_P = 2 s. Overall, the difference between SO and SFS is less than 15% for all soil profiles and pulse periods considered with no dependence on T_P or the soil profile.

For the soil profiles with H_s = 20 and 60 m, the SO and SOR models results in similar (less than 10% difference) peak shear demands for $T_P \geq 1.5$ s [see Figure 10] with less than 26% difference for $T_P \leq 1.0$ s; the SFS model computed 1.3 to 1.4 times more base shear than the SO model at T_P = 2.5 s with less than 26% difference for all other pulse periods. For the soil profiles with H_s = 140 and 220 m, the peak base shear computed from the SFS and SO models are between 0.45 to 0.8 times that of the SOR model for T_P = 1.5 – 2.5, with as much as 2.2 times the peak base shear of the SOR model for T_P = 3.0 – 4.0 s. For the computed peak base shear of all models, spurious shear spikes were computed at the base, which significantly influence the results for models that have drift ratio greater than 1% (see the section titled *Limitations*).

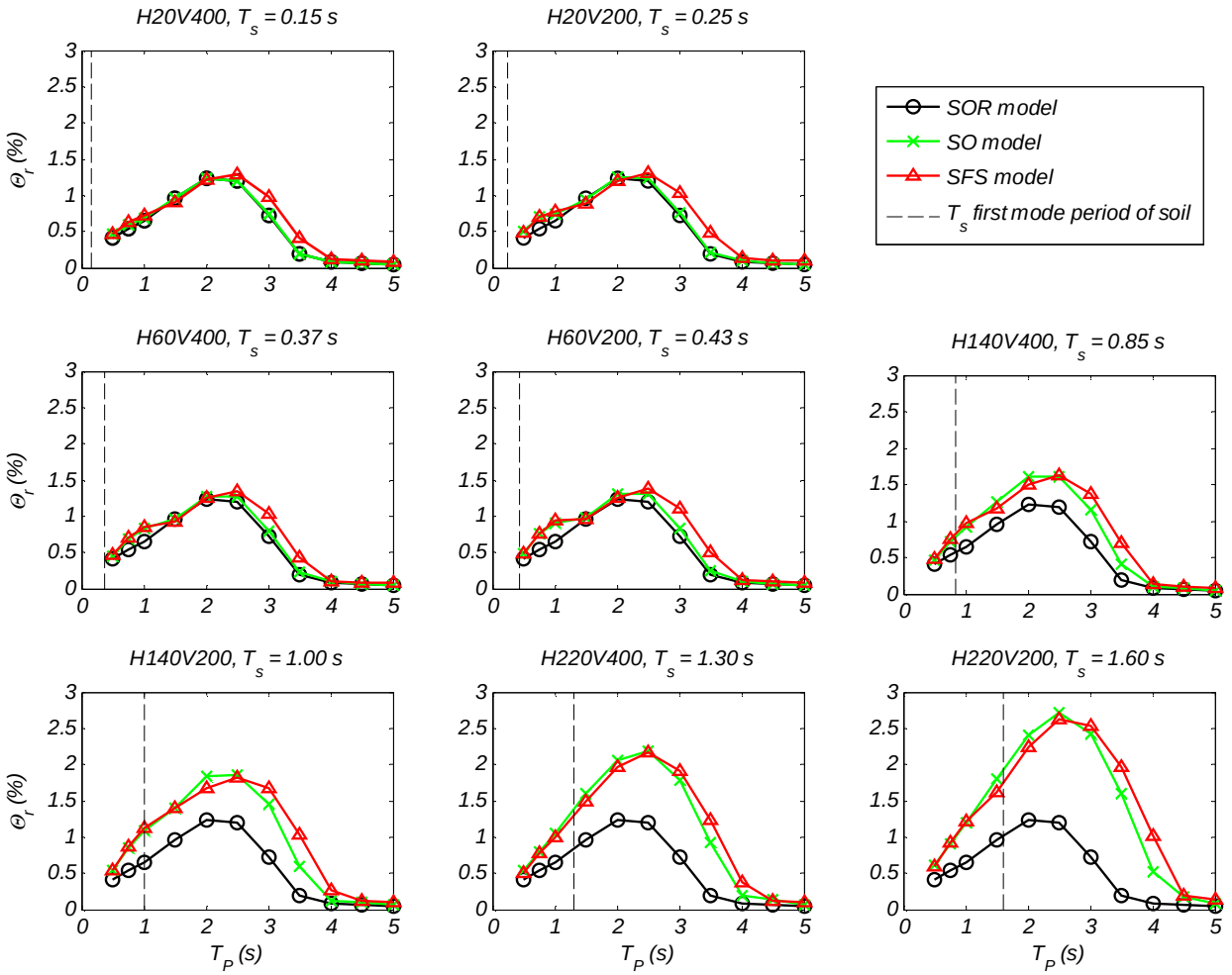

Figure 8. Peak roof drift ratio Θ_r for the structure-on-rock (SOR), structure-only (SO), and soil-foundation-structure (SFS) models corresponding to each of the 8 site cases considered.

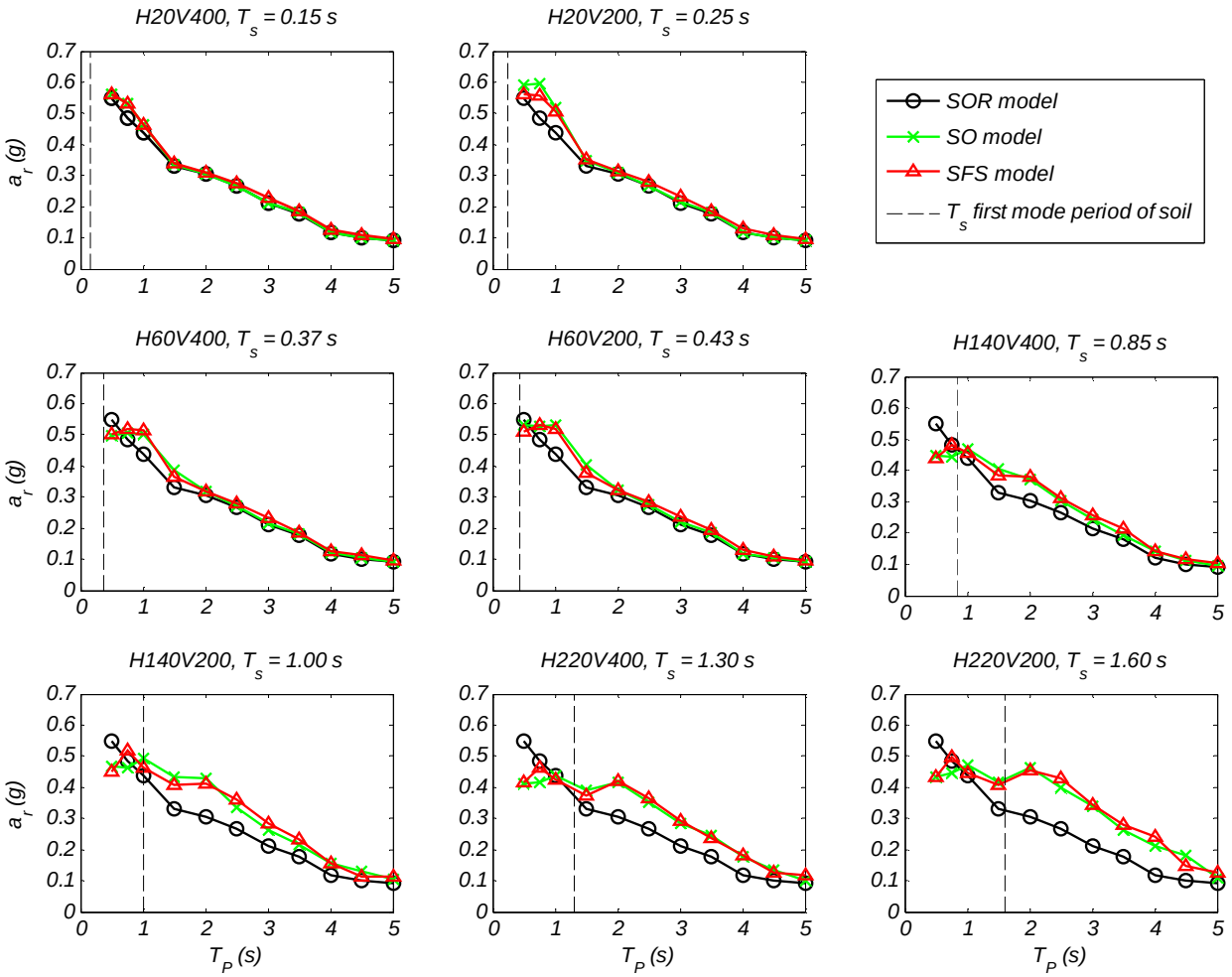

Figure 9. Peak roof acceleration a_r for the structure-on-rock (SOR), structure-only (SO), and soil-foundation-structure (SFS) models corresponding to each of the 8 site cases considered, filtered with low-pass at 5 Hz.

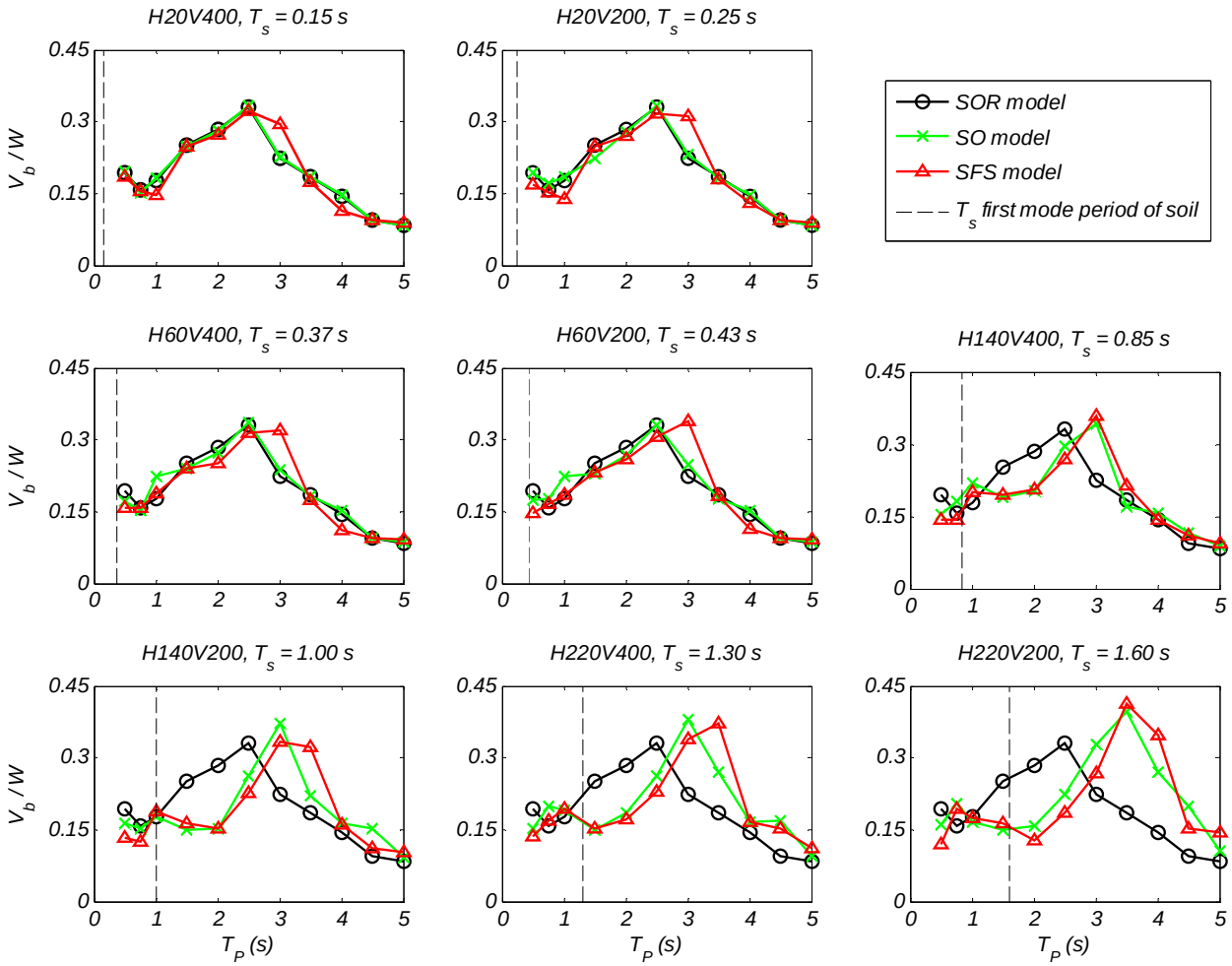

Figure 10. Peak base shear V_b normalized by super-structure weight W for the structure-on-rock (SOR), structure-only (SO), and soil-foundation-structure (SFS) models corresponding to each of the 8 site cases considered, filtered with low-pass at 5 Hz.

Limitations of the Models

This section describes the main limitations of the models used in this study. First, the seismic excitation of the models is assumed to consist of only vertically propagating shear waves from the bedrock – the model does not consider other incident angles or the case of seismic motion propagating from the sides of the model. In addition, the applied seismic excitation is assumed to have no spatial variability (thus, assuming the entire domain is shaken with the same motion at the same time).

The boundary conditions imposed for the models in the report reflect the case of an unbounded uniform soil layer above an elastic bedrock halfspace. This assumption is valid only for sites with relatively uniform soil.

The soil material model used is pressure-independent and thus does not account for the instantaneous confinement effects on the soil during dynamic nonlinear site response. The foundation-soil interface is rudimentary and does not allow for detach of the foundation from the soil. Due to the pressure-independent soil model, the soil has non-negligible strength in tension reducing the added flexibility due to SFSI.

Finally, it was observed that all models with the beam-column super-structure (SO, SSI, and SOR) have local spikes in the base shear time history, as shown in Figure 11. These local spikes occur for the models with relatively large roof displacement ratio (and thus large nonlinearity). As shown in Figure 11, these spikes occur when the structure reaches around zero displacement and may be related to a high frequency mode caused by sudden regain of stiffness during rocking. However, the shear spikes are shown to have period around 0.3 s, and thus is not completely filtered out in the results presented in this paper; this accounts partially for the increase of peak base shear response [shown in Figure 10] for input pulses of period T_P = 1.5 – 3 s for SOR and SO and SFS with soil profiles with H_s = 20 and 60 m, and T_P = 2.5 – 4 s for SO and SFS with soil profiles with H_s = 140 and 220 m.

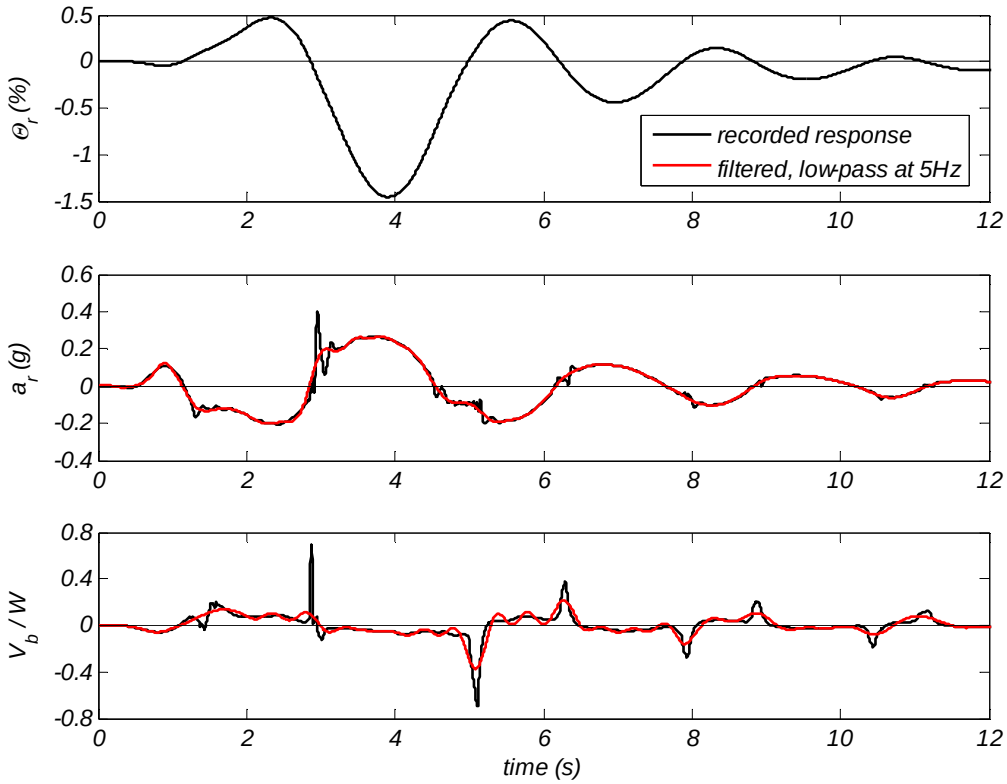

Figure 11. Roof drift ratio, roof acceleration, and normalized base shear time history for the structure-only (SO) model with soil profile Vs200-140m, subject to the T_P = 3.0 s pulse, showing the computed base shear spikes.

Conclusion

In this report, the effects of nonlinear site response and soil-foundation-structure interaction (SFSI) are studied for a 20-story core wall building with a caisson foundation. The building, including the subterranean levels and foundation, and the surrounding soil layer are modeled using 2D nonlinear 4-node finite elements and fiber-section beam-column elements. The soil is modeled using the Von Mises yield criterion with a hyperbolic backbone curve for the shear stress-strain relation. Nonlinear interface effects (such as gaps forming between soil and foundation) are not modeled. Eight soil site cases are considered with depth of soil H_s = 20, 60, 140, and 220 m and shear wave velocity at the top of the soil layer $V_{s,top}$ = 200 and 400 m/s with linear increase with depth; the first modal period of the soil layers T_s ranged from 0.15 s to 1.6 s. The imposed motion at the base of the soil layer is a single cycle acceleration pulse with dominant period varying between 0.5 and 5.0 s in order to approximate the pulse-like nature of strong near-fault ground motions.

To study the two effects separately, the following models are used: (1) free-field soil, consisting of only the soil (or rock) layer, (2) structure-only, consisting of only the super-structure model and subjected to imposed motion recorded from the top of the free-field soil models, and (3) soil-foundation-structure, which includes the entire structure, foundation, and surrounding soil layer. Based on the results, the following conclusions are drawn:

- De-amplification of acceleration occurs for pulses with period $T_P \leq 0.5$ s (for soil profile with H_s = 20 m) and $T_P \leq 1.0$ s (H_s = 220 m).
- Maximum amplification of peak velocity at soil surface varies from 1.1 (H_s = 20 m) to 1.6 (H_s = 220 m) times the peak velocity of the rock motions, occurring for pulse excitation with period of 0.75 and 2.0 s, respectively. Maximum peak acceleration and velocity computed for soil profiles with $V_{s,top}$ = 200 m/s resulted up to 1.16 times that computed for soil profiles with $V_{s,top}$ = 400 m/s.
- Soil profiles with H_s = 220 m resulted in a period elongation of the excitation pulse at the surface of the soil layer for pulses with $T_P \leq 1.0$ s. For those cases, the maximum value of spectral displacement (Sd) occurs at an oscillator period between T_s (equal to 1.3 and 1.6 s for the soil profile with $V_{s,top}$ = 200 and 400 m/s, respectively) and 2.0 s.
- When decomposed from the nonlinear site effect, SFSI has small (less than 8% difference) effect on the peak roof drift ratio for the 20-story building (cracked period of 2.0 s) for an

imposed pulse with period $T_P \leq 2.5$ s (for H_s = 20, 60, and 140 m) and $T_P \leq 3.0$ s (for H_s = 220 m). SFSI also has a small effect (less than 7% difference) on the maximum value of peak roof drift ratio. However, for pulses with $3.0 \leq T_P \leq 3.5$ s (for H_s = 20, 60, and 140 m) and $3.5 < T_P < 4.0$ s (for H_s = 220 m), the peak roof drift ratio of the structure accounting for SFSI at a pulse period of T_P corresponds to that of the structure-only model at a pulse period of (T_P – 0.25 s), resulting in a peak roof drift ratio of a maximum of 2.3 times that of the structure-only model.

- When decomposed from the nonlinear site effect, the SFSI effect on peak roof acceleration is small (an average difference of 0.013 g and maximum of 0.055 g) with no dependence on T_P or the soil profile. Spurious shear spikes were computed at the base around zero displacement of the super structure, which affected the computed peak base shear values for models that had drift ratio greater than 1%.

Acknowledgements

The first author was supported from the France Berkeley Fund program for this work.

References

Calugaru, V., and Panagiotou, M. (2012a). "Response of tall cantilever wall buildings to strong pulse type seismic excitation." *Earthquake Engineering & Structural Dynamics*, 41(9), 1301–1318.

Calugaru, V., and Panagiotou, M. (2012b). "Seismic responses of 20-story base-isolated and fixed-base RC structural wall buildings subjected to near-fault ground shaking." Report No. UCB/SEMM-2012/03, Earthquake Engineering Research Center, University of California, Berkeley.

Elgamal, A., Yan, L., Yang, Z., and Conte, J. P. (2008). "Three-dimensional seismic response of Humboldt Bay bridge-foundation-ground system." *Journal of Structural Engineering*, 134(7), 1165–1176.

Gazetas, G. (1991). "Formulas and charts for impedances of surface and embedded foundations." *Journal of Geotechnical Engineering*, 117(9), 1363–1381.

Gerolymos, N., and Gazetas, G. (2006). "Development of Winkler model for static and dynamic response of caisson foundations with soil and interface nonlinearities." *Soil Dynamics and Earthquake Engineering*, 26(5), 363–376.

Hall, J. F., Heaton, T. H., Halling, M. W., and Wald, D. J. (1995). "Near-source ground motion and its effects on flexible buildings." *Earthquake Spectra*, 11, 569–606.

Jeremić, B., Jie, G., Preisig, M., and Tafazzoli, N. (2009). "Time domain simulation of soil–foundation–structure interaction in non-uniform soils." *Earthquake Engineering & Structural Dynamics*, 38(5), 699–718.

List of tallest buildings in Christchurch. (n.d.). In *Wikipedia*. Retrieved August, 6 2013, from http://en.wikipedia.org/wiki/List_of_tallest_buildings_in_Christchurch

Lu, Y., and Panagiotou, M. (2013). "Characterization and representation of pulse-like ground motions using cumulative pulse extraction via wavelet analysis," Report No. UCB/SEMM-2013/01, Earthquake Engineering Research Center, University of California, Berkeley.

Mavroeidis, G. P., and Papageorgiou, A. S. (2003). "A mathematical representation of near-fault ground motions." *Bulletin of the Seismological Society of America*, 93(3), 1099–1131.

McKenna, F., Fenves, G. L., Scott, M. H., and Jeremić, B. (2000). "Open system for earthquake engineering simulation." <http://opensees.berkeley.edu>

Mylonakis, G., and Gazetas, G. (2000). “Seismic soil-structure interaction: beneficial or detrimental?” *Journal of Earthquake Engineering*, 4(3), 277–301.

Rodriguez-Marek, A., and Bray, J. D. (2006). “Seismic site response for near-fault forward directivity ground motions.” *Journal of Geotechnical and Geoenvironmental Engineering*, 132(12), 1611–1620.

Seed, H. B., Ugas, C., and Lysmer, J. (1976). “Site-dependent spectra for earthquake-resistant design.” *Bulletin of the Seismological Society of America*, 66(1), 221–243.

Somerville, P., and Graves, R. (1993). “Conditions that give rise to unusually large long period ground motions.” *The Structural Design of Tall Buildings*, *2*(3), 211–232.

Stewart, J. P., and Tileylioglu, S. (2007). “Input ground motions for tall buildings with subterranean levels.” *The Structural Design of Tall and Special Buildings*, 16(5), 543–557.

Unchs (2001). “Urban millennium.” United Nations Centre for Human Settlements Report, p.2. New York, June 2001.

Wood, A. (2007). “Sustainability: a new high-rise vernacular?” *The Structural Design of Tall and Special Buildings*, 16(4), 401–410.

Zhang, Y., Yang, Z., Bielak, J., Conte, J. P., and Elgamal, A. (2003). “Treatment of seismic input and boundary conditions in nonlinear seismic analysis of a bridge ground system.” *16th ASCE Engineering Mechanics Conference*, University of Washington, Seattle, 16–18 July 2003.

Zhang, Y., Conte, J. P., Yang, Z., Elgamal, A., Bielak, J., and Acero, G. (2008). “Two-dimensional nonlinear earthquake response analysis of a bridge-foundation-ground system.” *Earthquake Spectra*, 24(2), 343–386.

Appendix A: Acceleration and velocity time history and spectral displacement (2% damping) for the motions computed at the free-surface of the free-field rock (FFR) model compared with that of the free-field soil (FFS) model for each of the soil sites.

Soil site profile H20V400 – T_s = 0.15 s

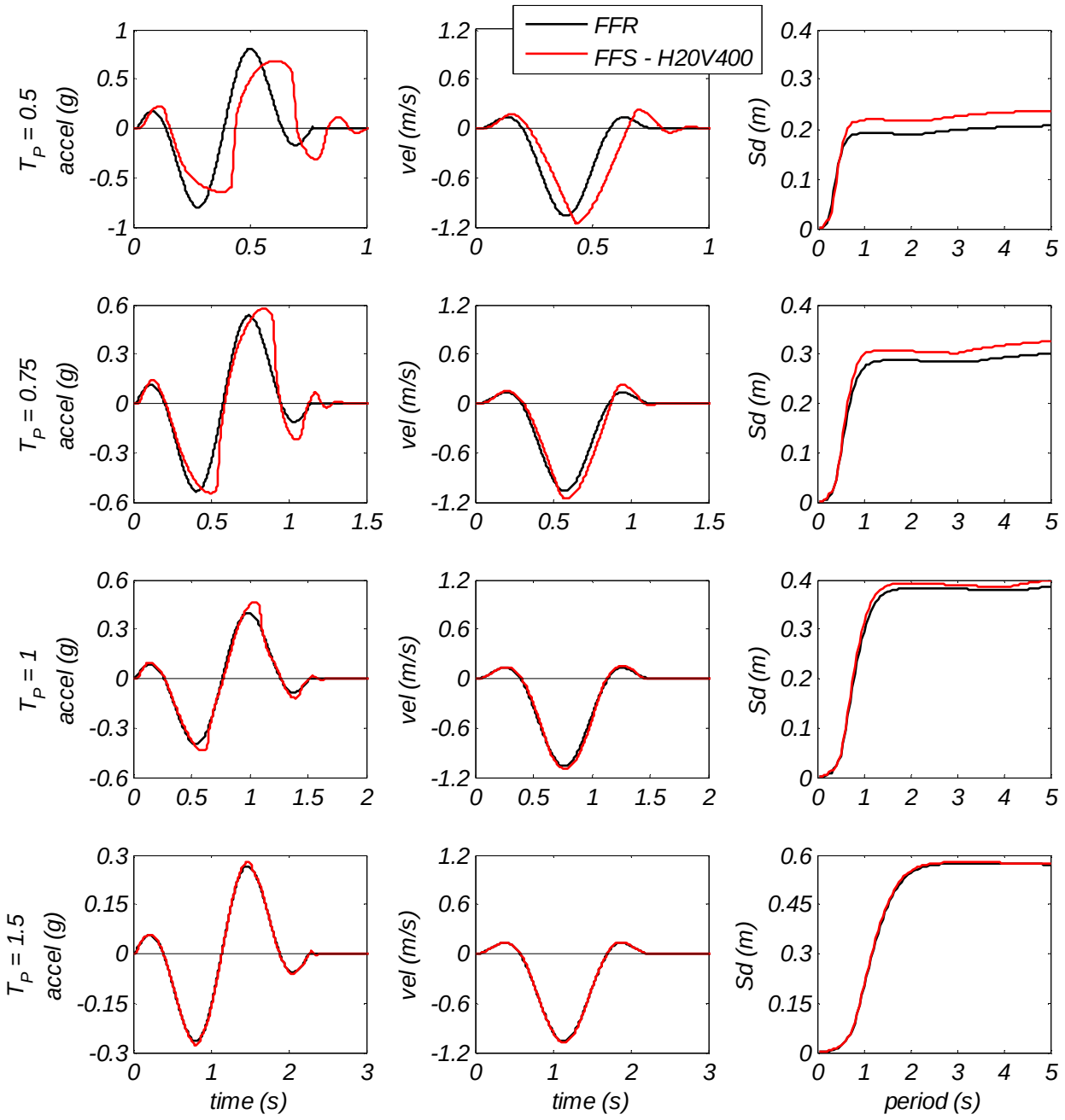

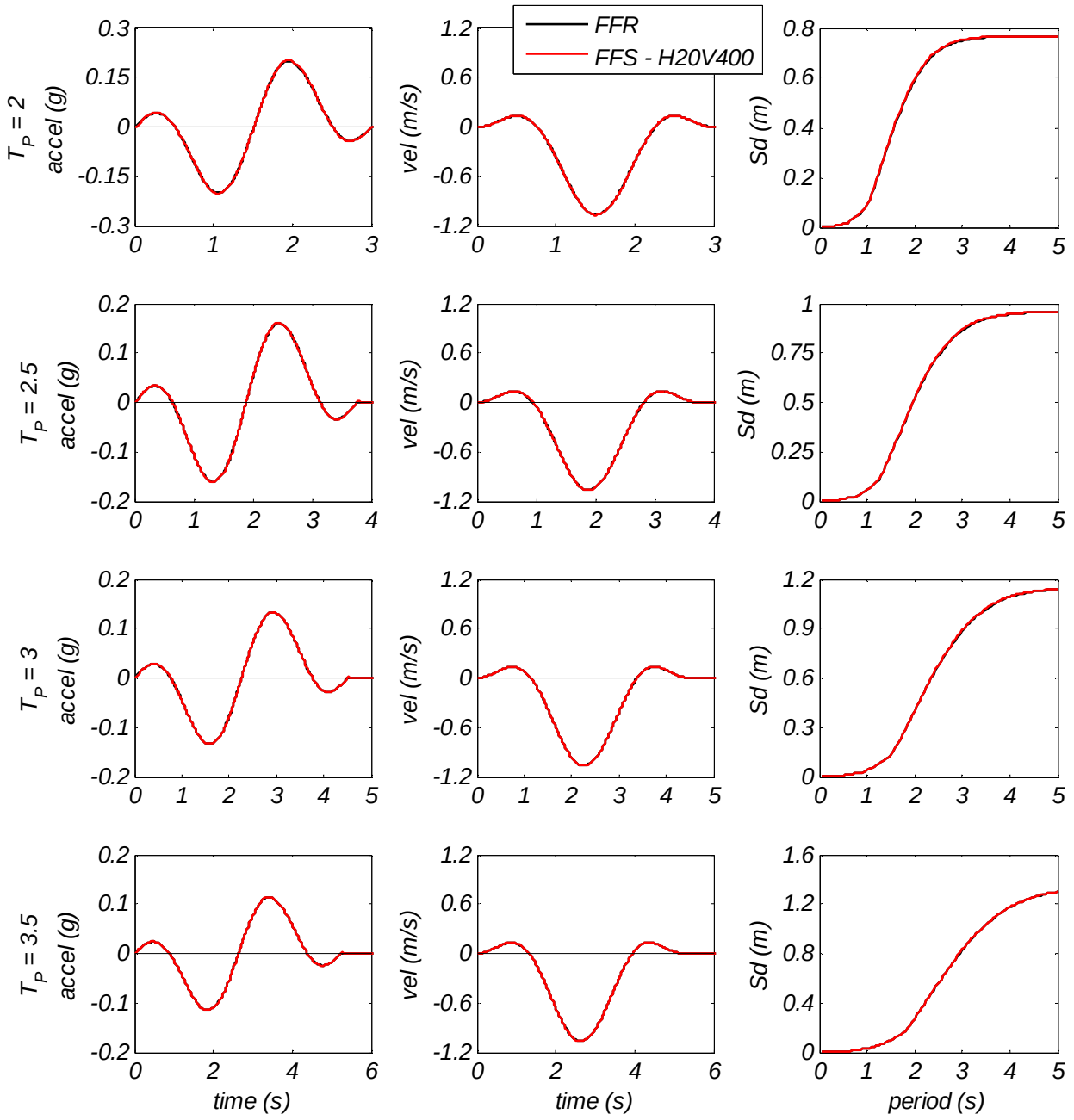
FFR
FFS - H20V400
T_P = 2
T_P = 2.5
T_P = 3
T_P = 3.5
accel (g)
vel (m/s)
Sd (m)
time (s)
time (s)
period (s)

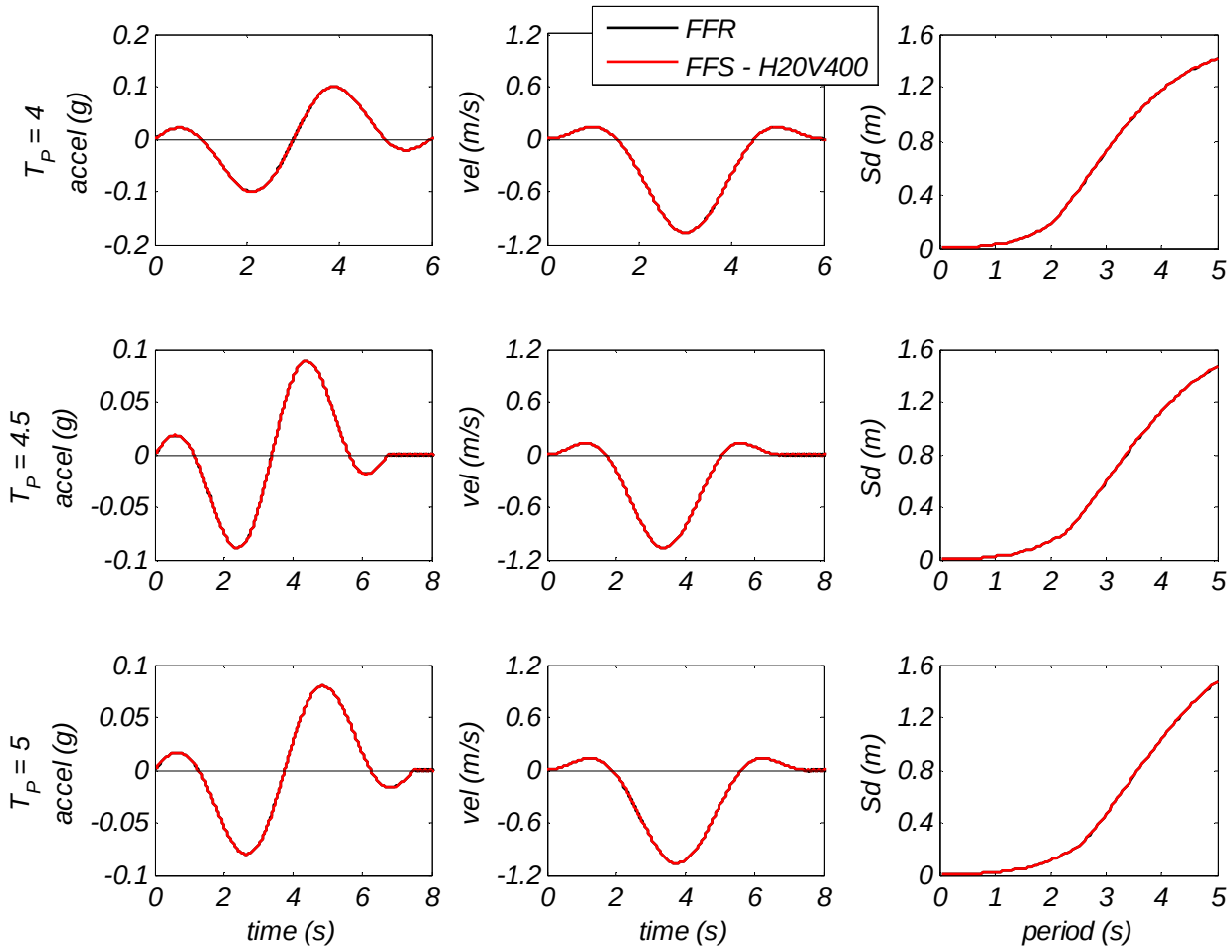
FFR
FFS - H20V400
T_P = 4
T_P = 4.5
T_P = 5
accel (g)
vel (m/s)
Sd (m)
time (s)
time (s)
period (s)

Soil site profile H20V200 – T_s = 0.25 s

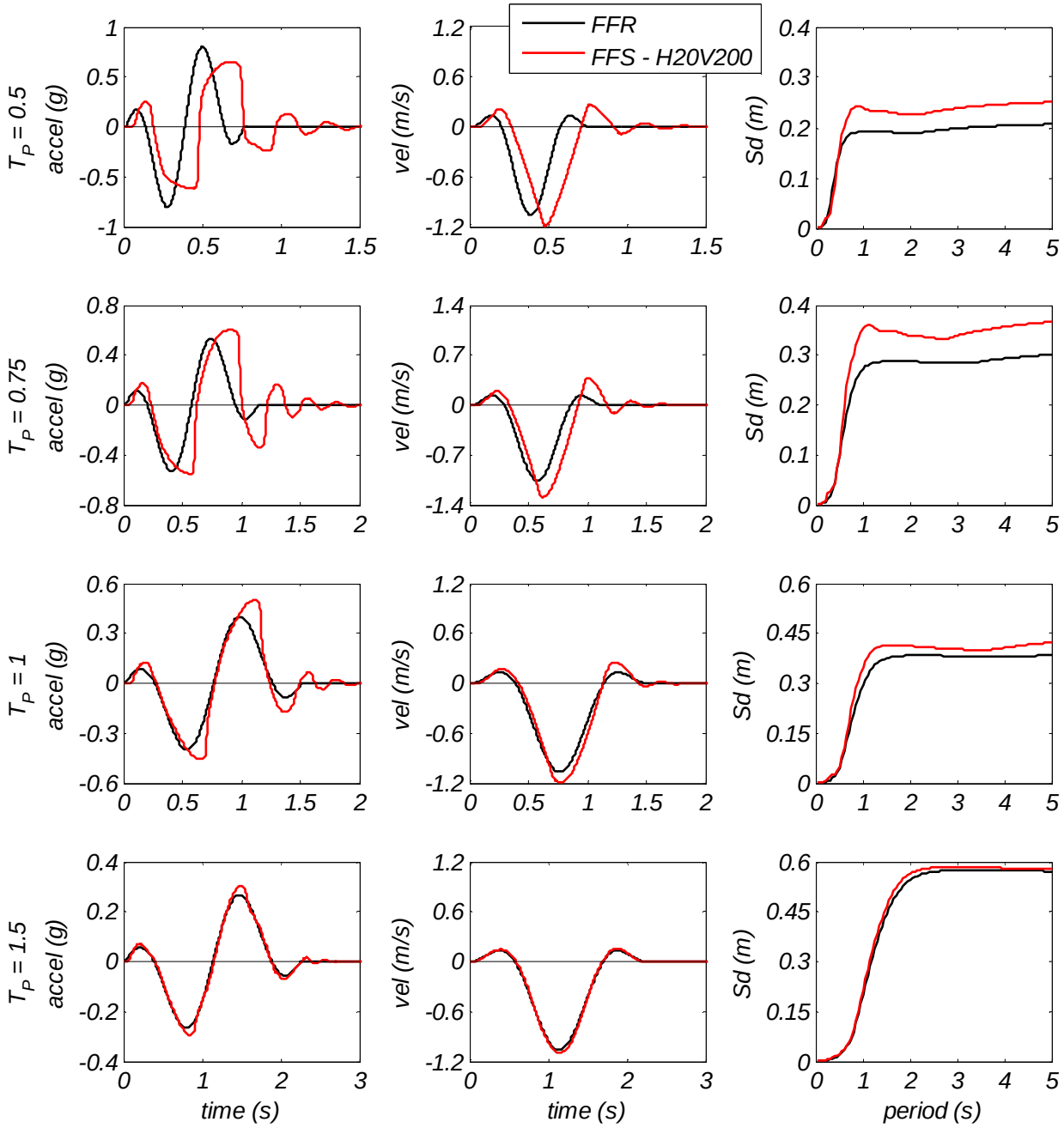

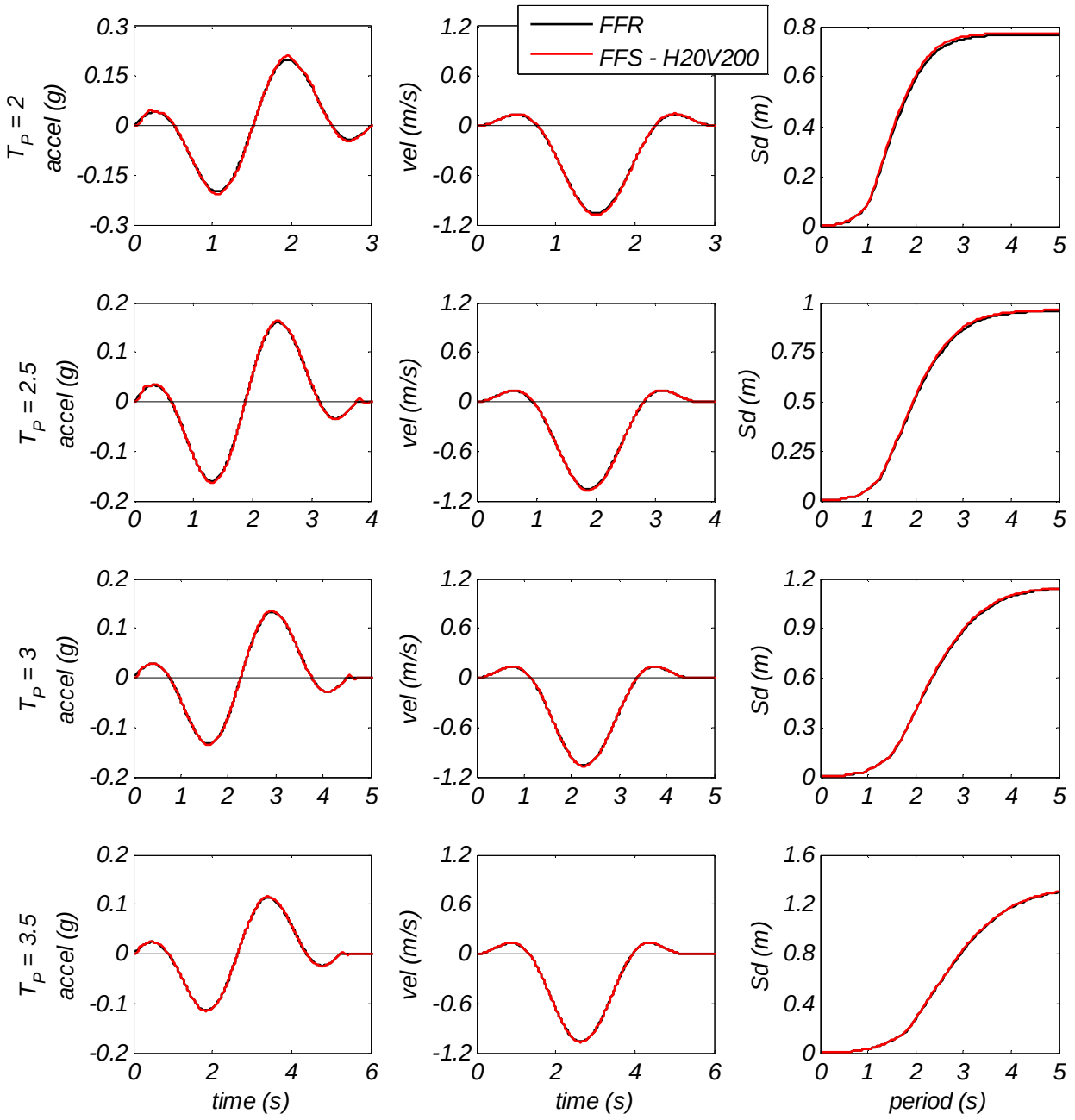
FFR
FFS - H20V200
T_P = 2
T_P = 2.5
T_P = 3
T_P = 3.5
accel (g)
vel (m/s)
Sd (m)
time (s)
time (s)
period (s)

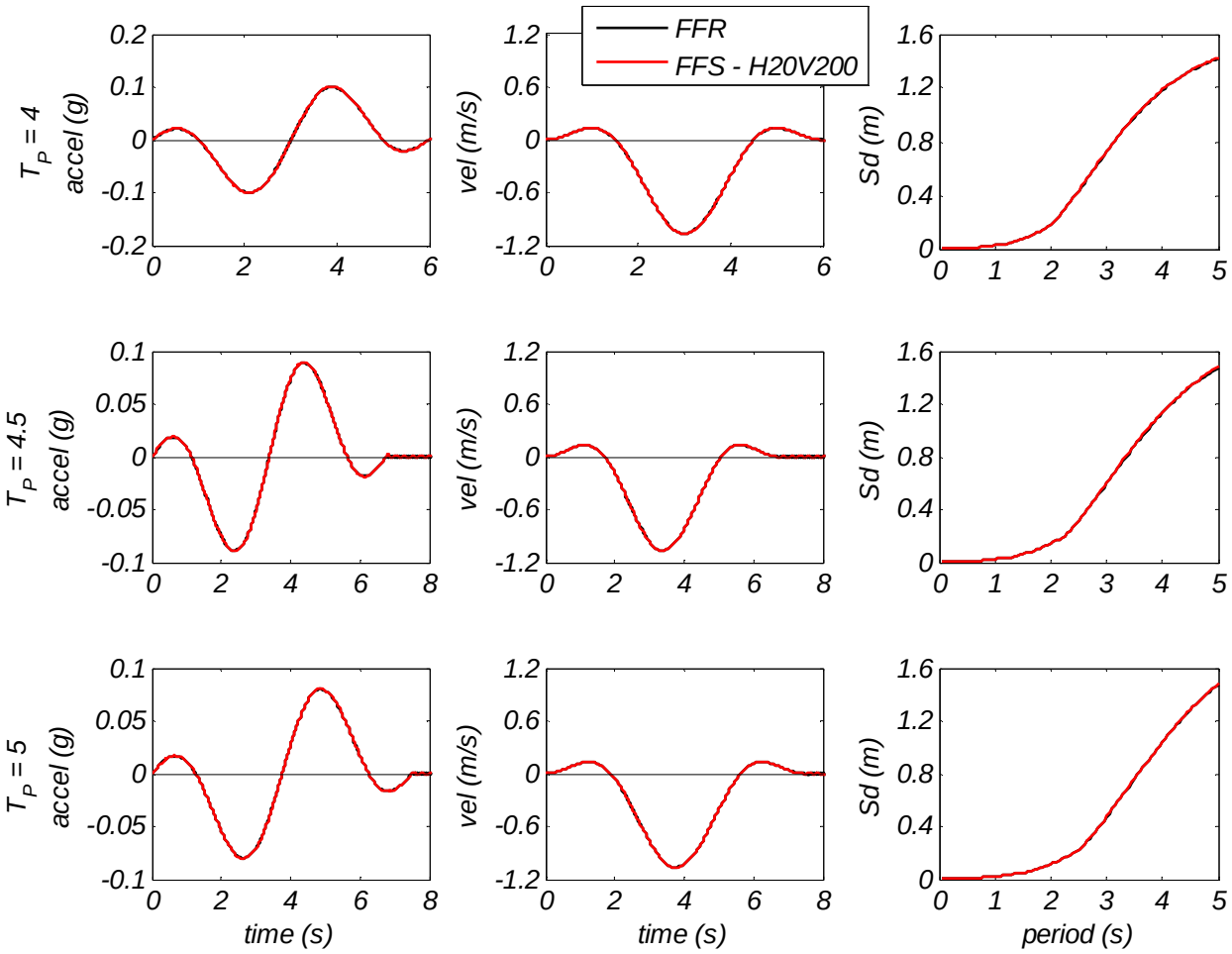
FFR
FFS - H20V200
T_P = 4
T_P = 4.5
T_P = 5
accel (g)
vel (m/s)
Sd (m)
time (s)
time (s)
period (s)

Soil site profile H60V400 – T_s = 0.37 s

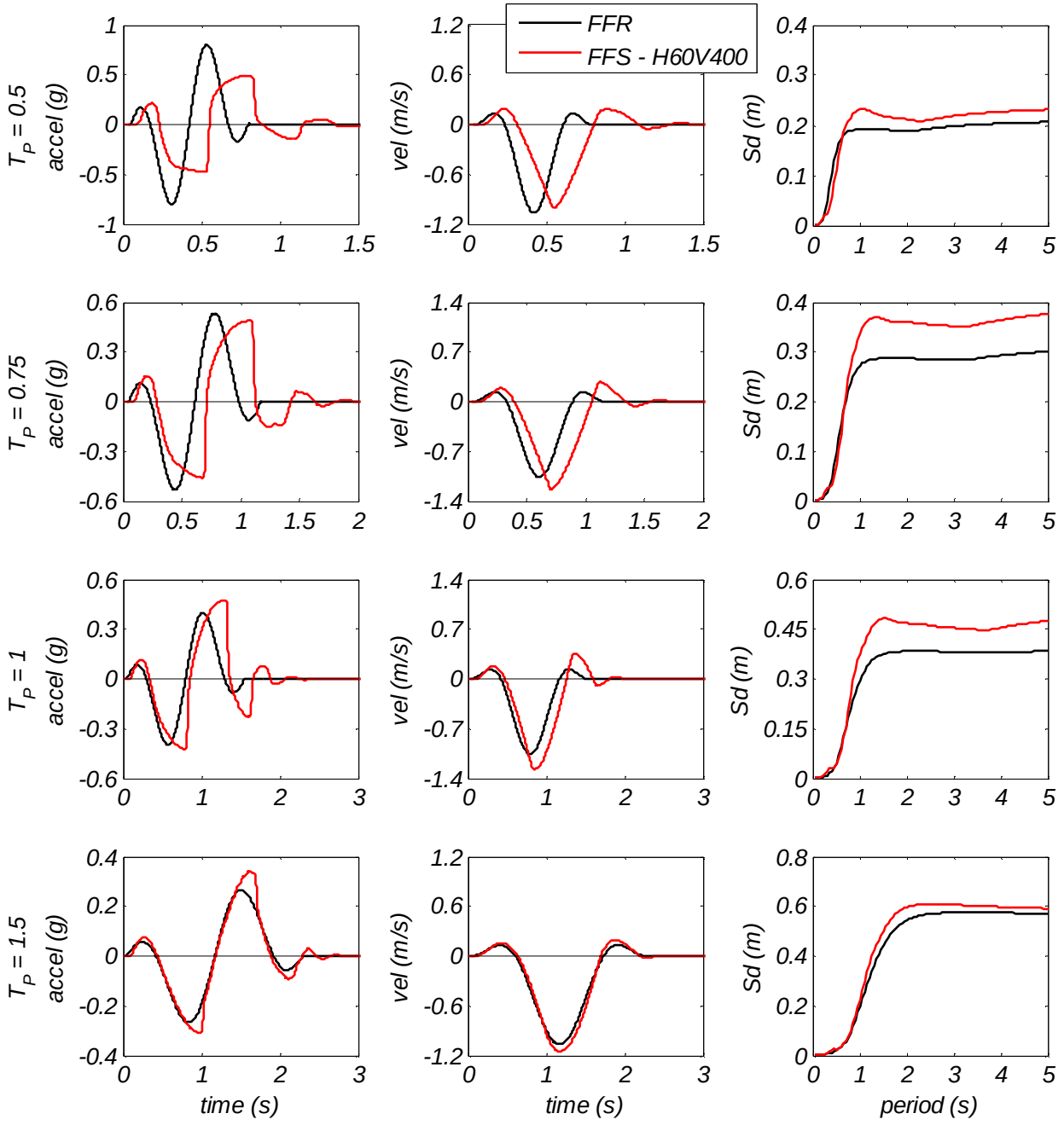

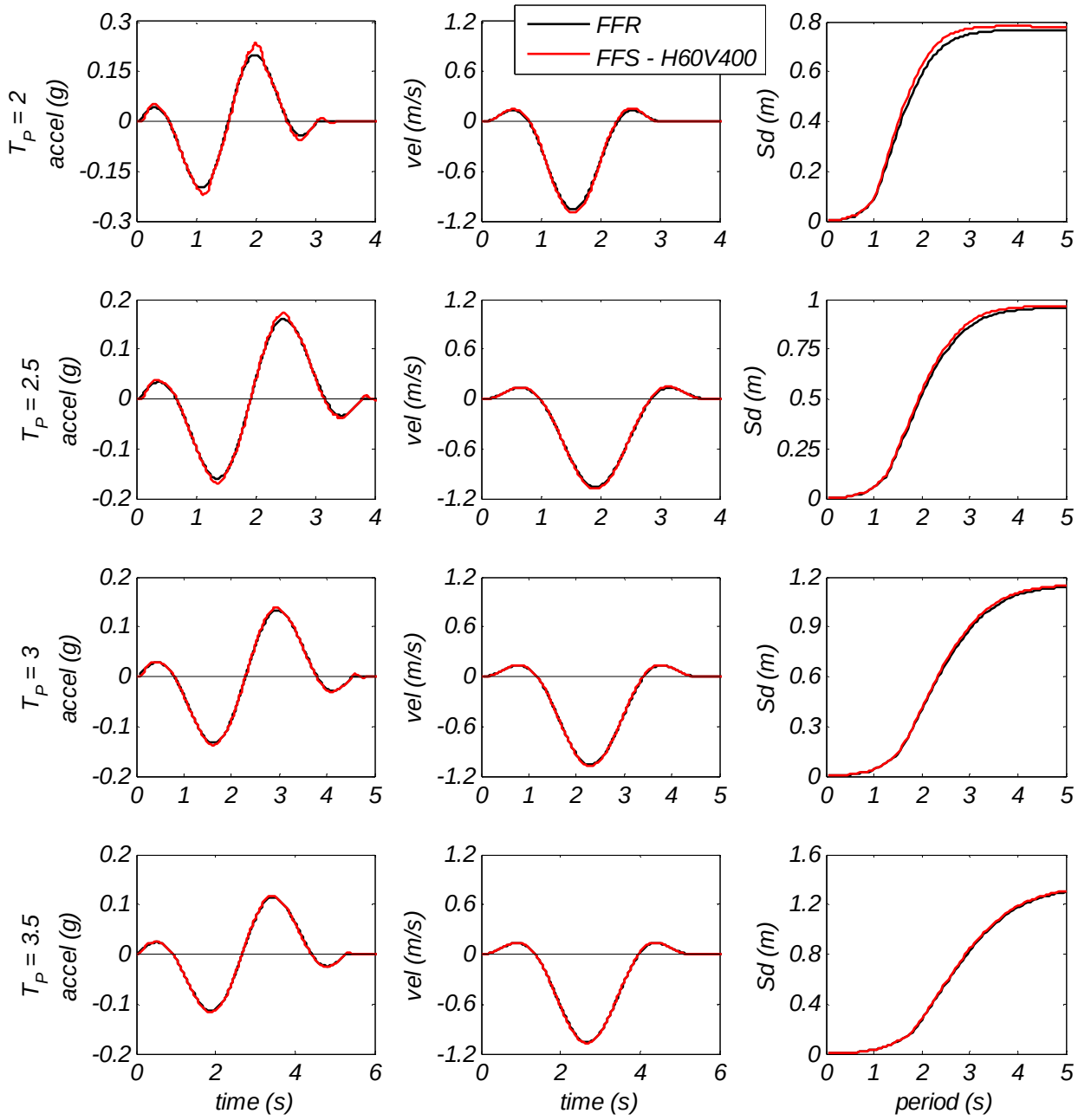
FFR
FFS - H60V400
T_P = 2
T_P = 2.5
T_P = 3
T_P = 3.5
accel (g)
vel (m/s)
Sd (m)
time (s)
time (s)
period (s)

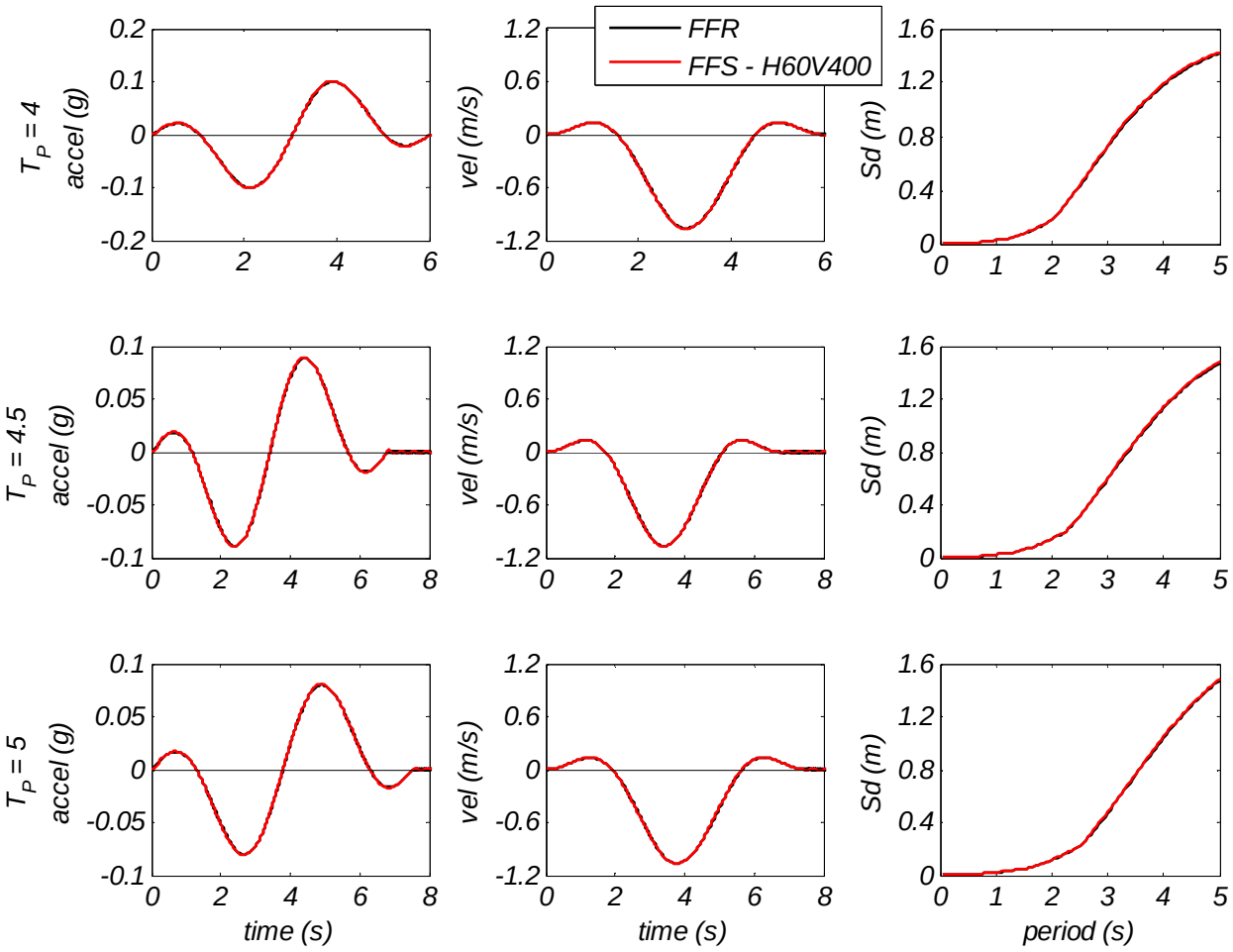
FFR
FFS - H60V400
T_P = 4
T_P = 4.5
T_P = 5
accel (g)
vel (m/s)
Sd (m)
time (s)
time (s)
period (s)

Soil site profile H60V200 – T_s = 0.43 s

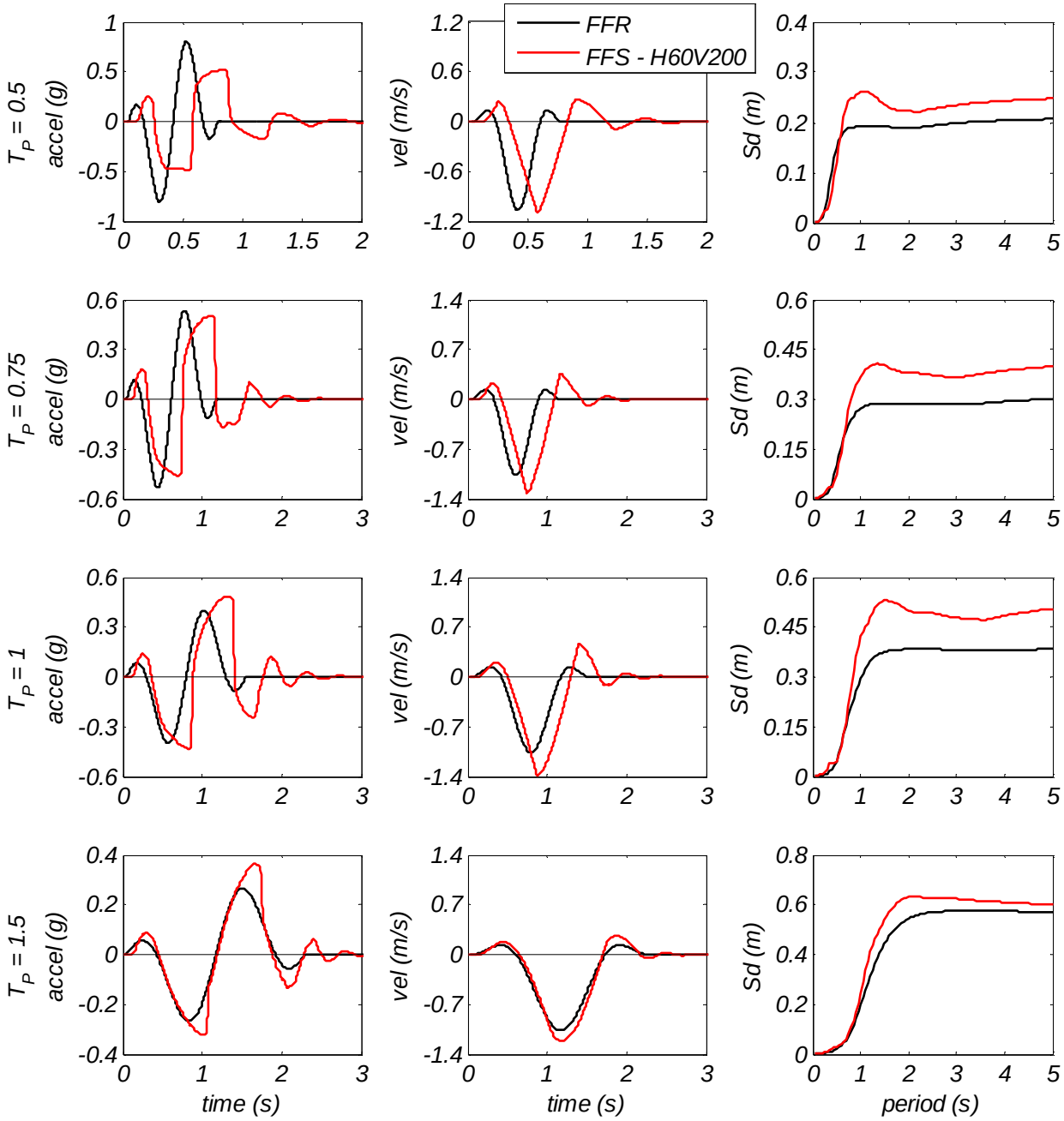

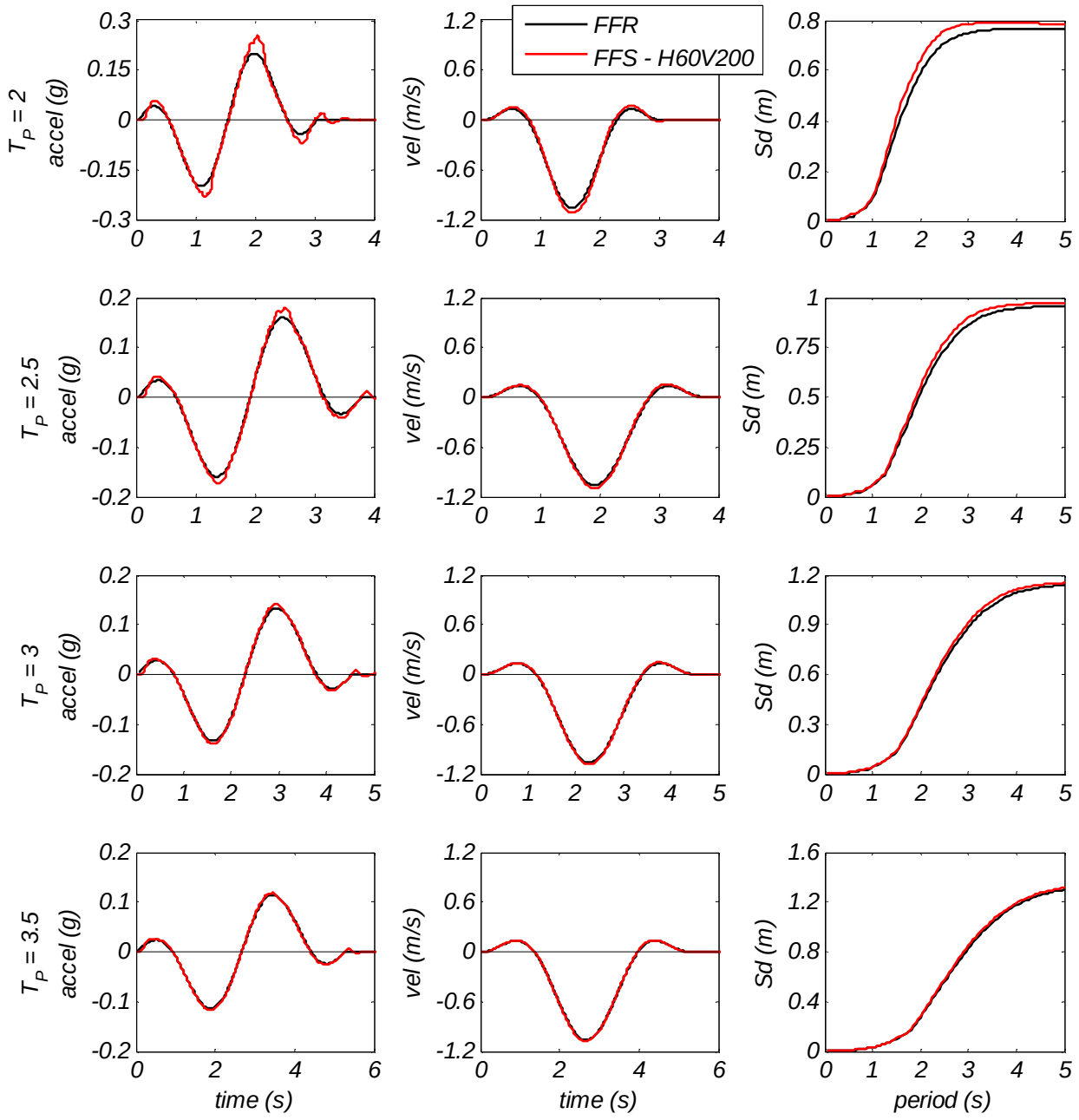
FFR
FFS - H60V200
T_P = 2
T_P = 2.5
T_P = 3
T_P = 3.5
accel (g)
vel (m/s)
Sd (m)
time (s)
time (s)
period (s)

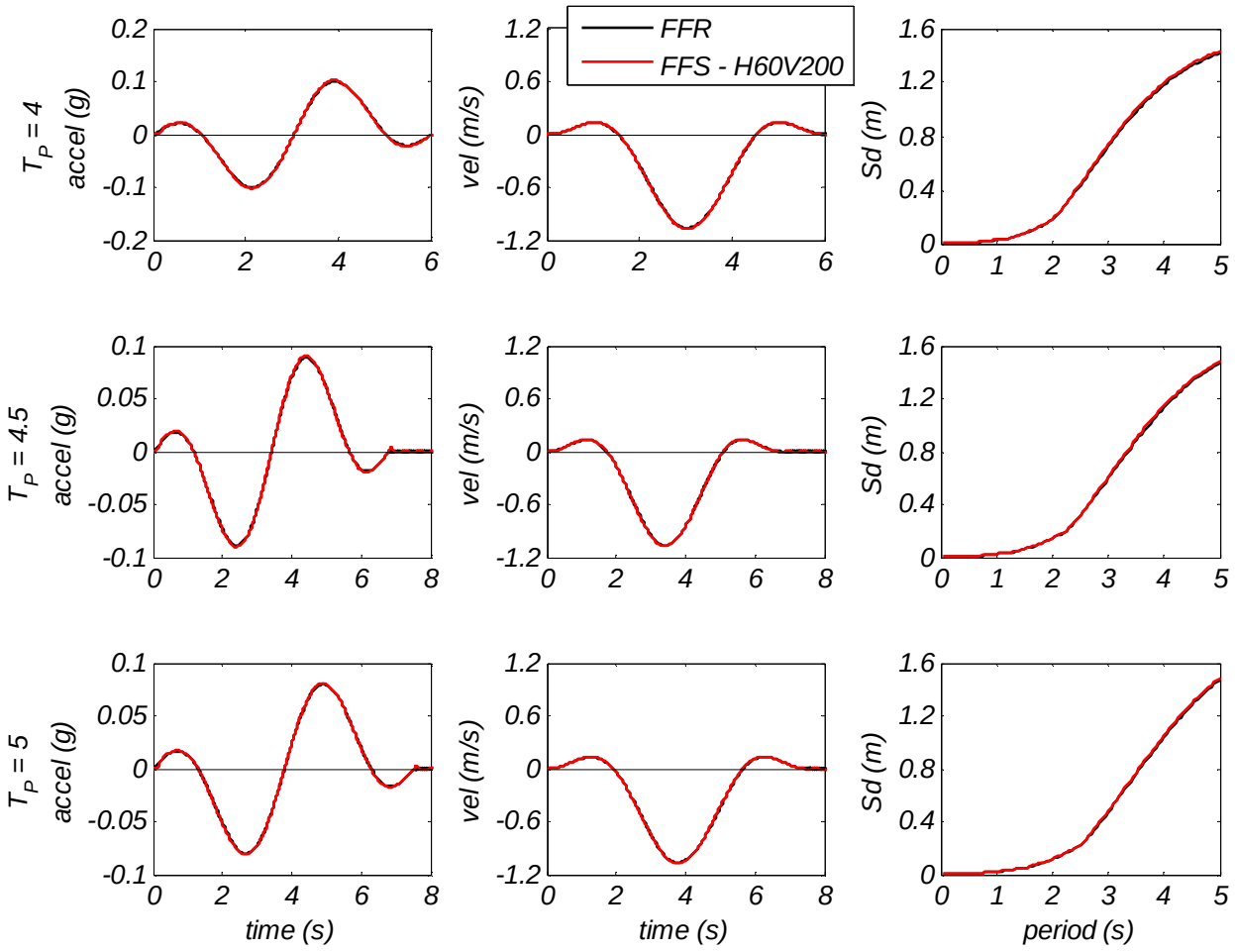
FFR
FFS - H60V200
T_P = 4
T_P = 4.5
T_P = 5
accel (g)
vel (m/s)
Sd (m)
time (s)
time (s)
period (s)

Soil site profile H140V400 – T_s = 0.85 s

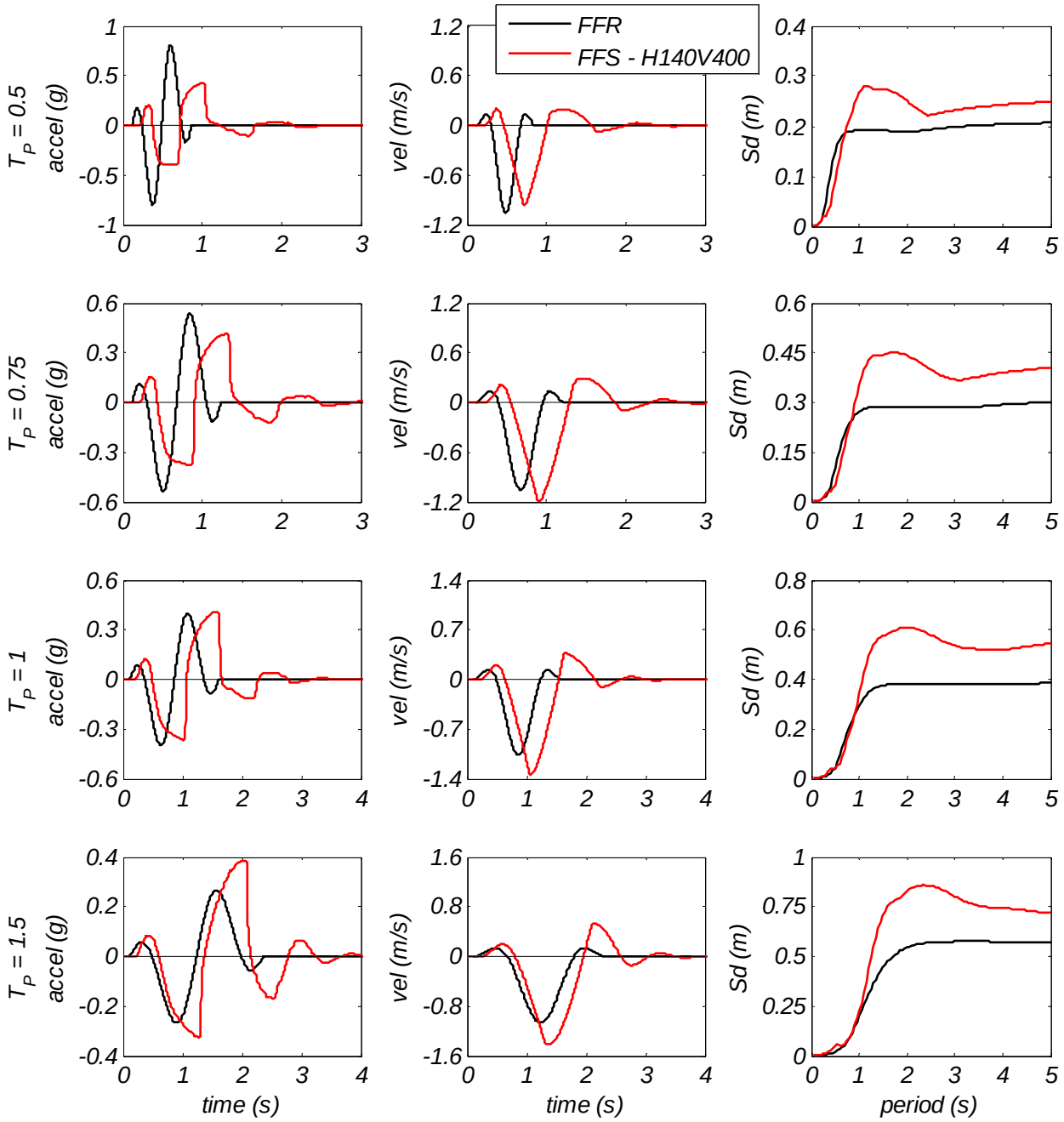

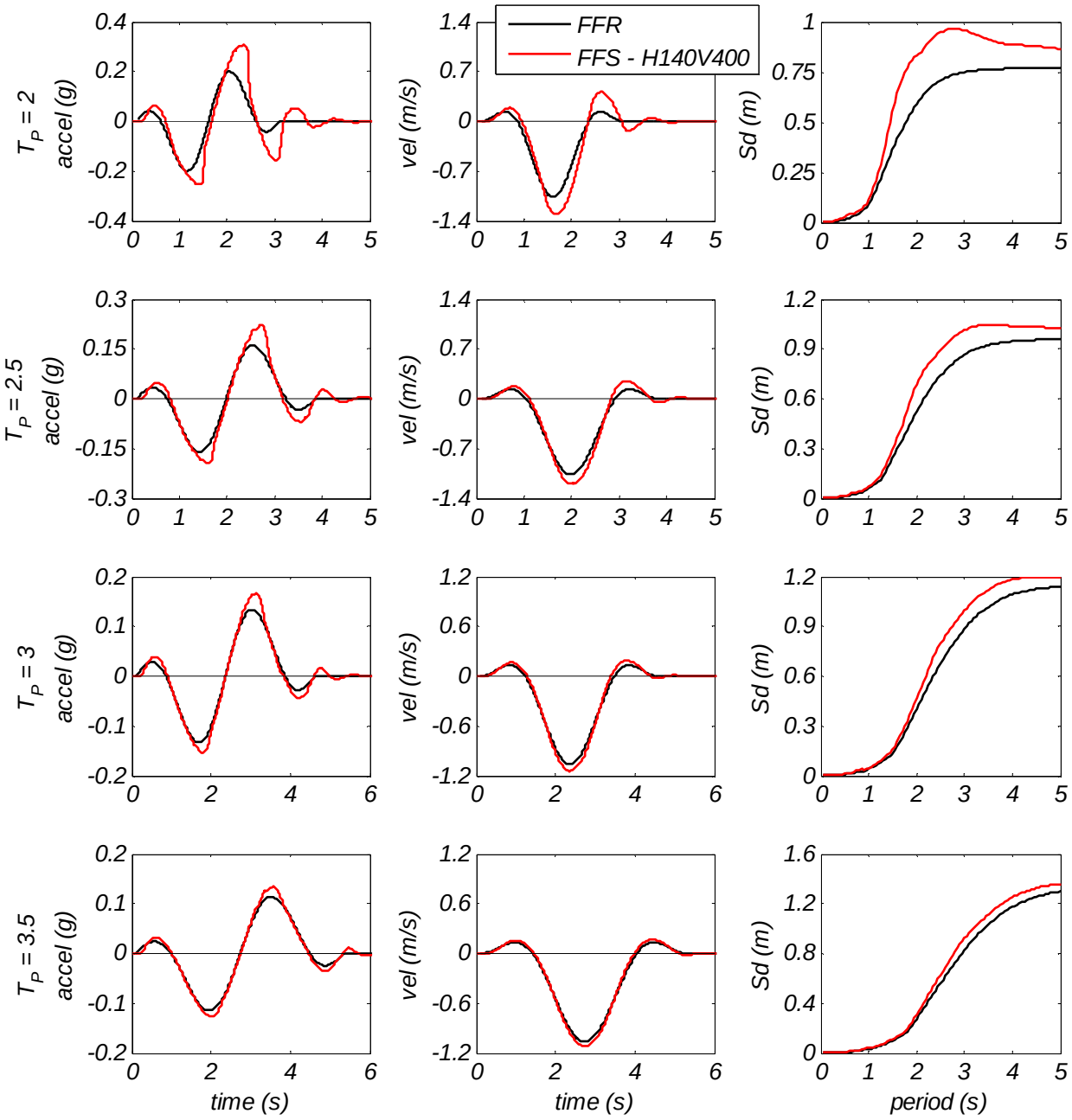
FFR
FFS - H140V400
T_P = 2
T_P = 2.5
T_P = 3
T_P = 3.5
accel (g)
vel (m/s)
Sd (m)
time (s)
time (s)
period (s)

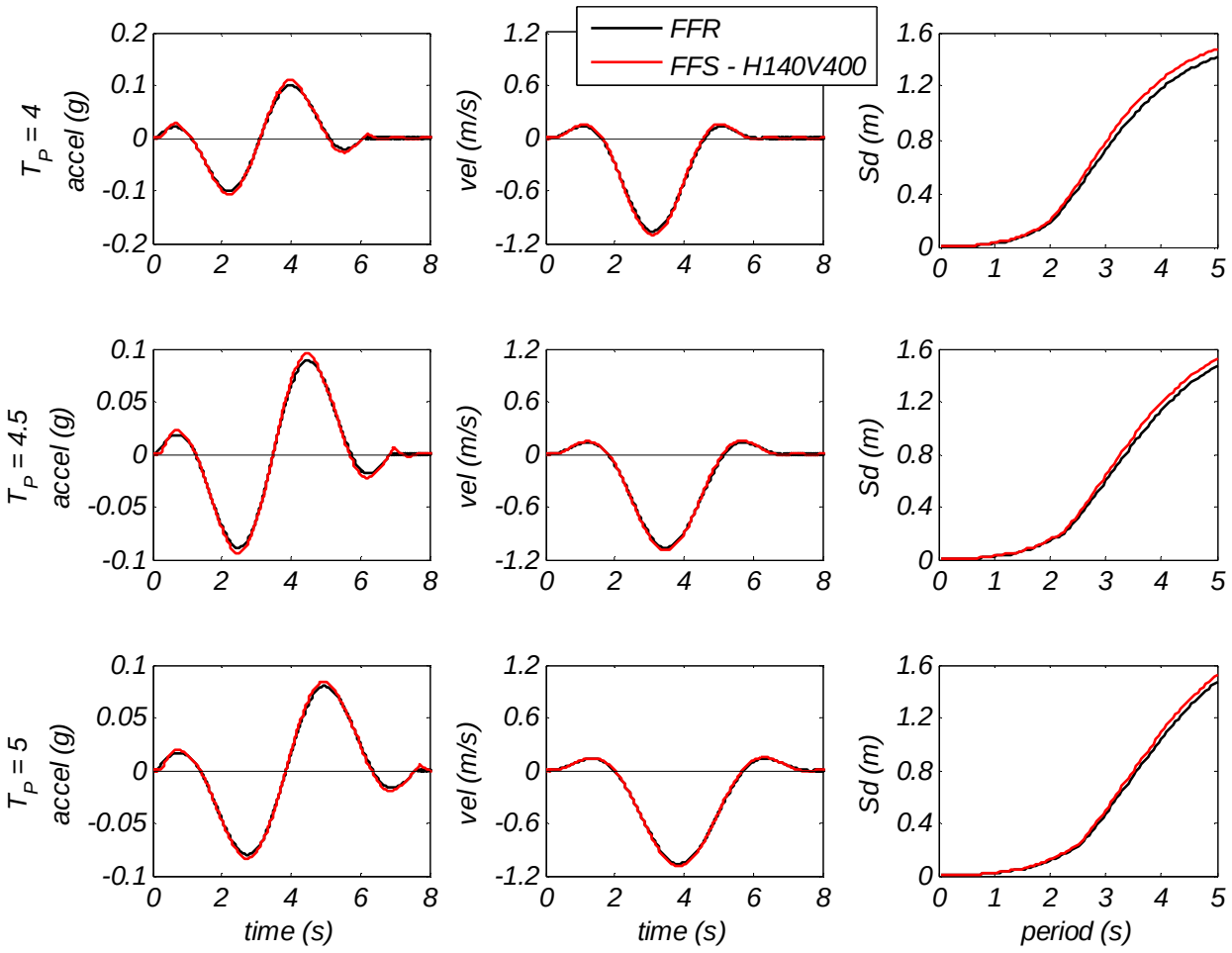
FFR
FFS - H140V400
T_P = 4
T_P = 4.5
T_P = 5
accel (g)
vel (m/s)
Sd (m)
time (s)
time (s)
period (s)

Soil site profile H140V200 – T_s = 1.0 s

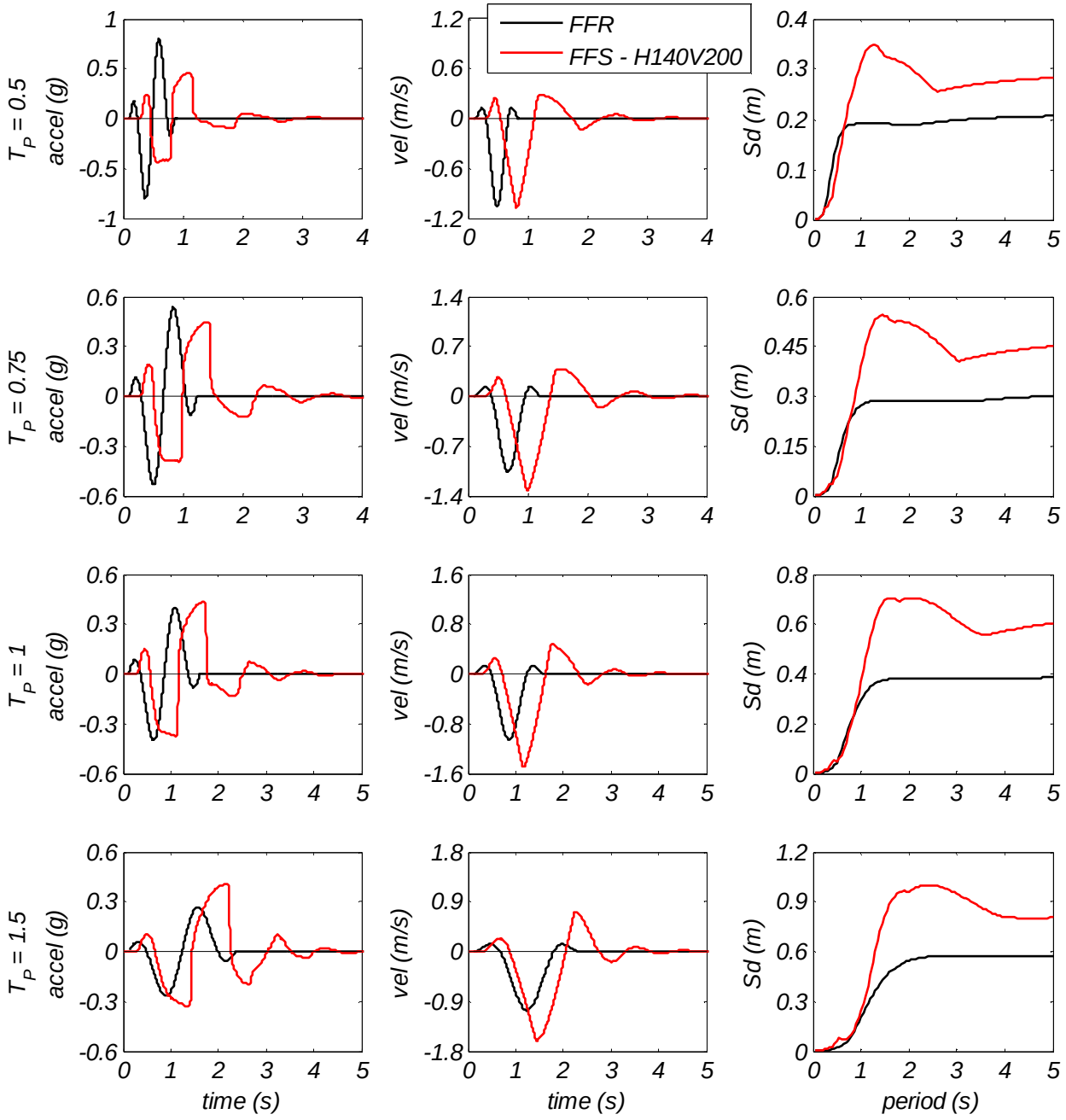

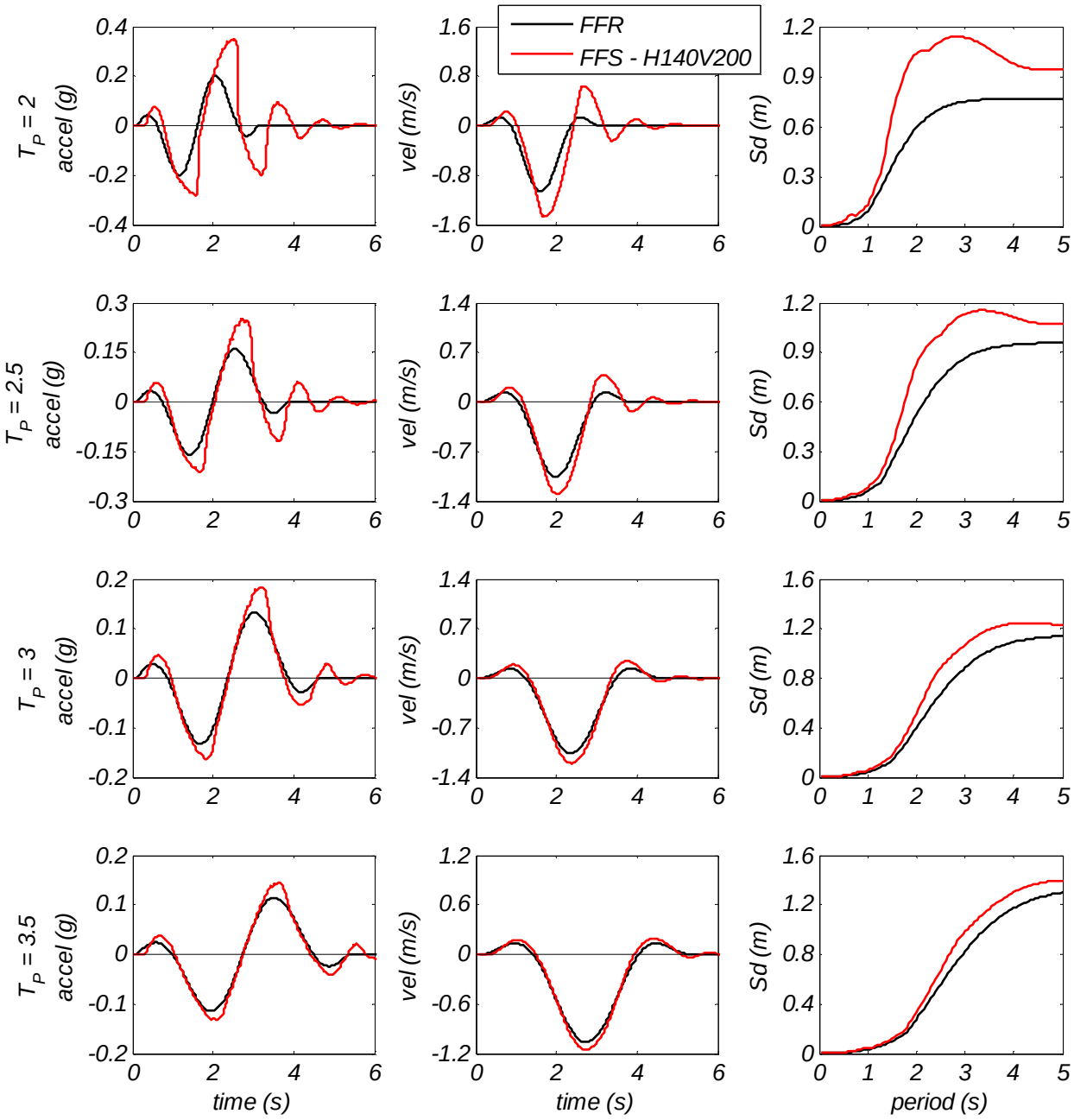
FFR
FFS - H140V200
T_P = 2
T_P = 2.5
T_P = 3
T_P = 3.5
accel (g)
vel (m/s)
Sd (m)
time (s)
time (s)
period (s)

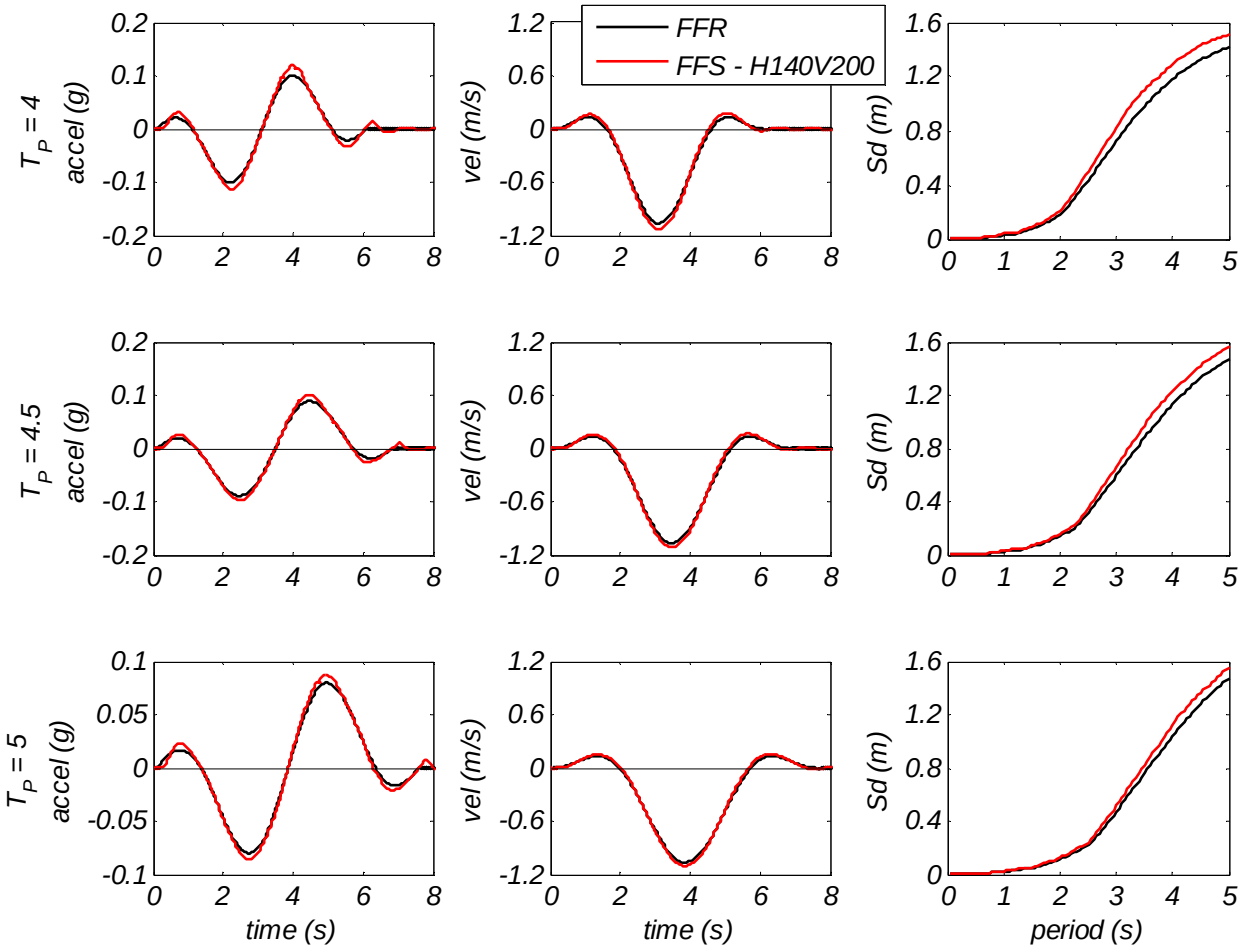
FFR
FFS - H140V200
T_P = 4
T_P = 4.5
T_P = 5
accel (g)
vel (m/s)
Sd (m)
time (s)
time (s)
period (s)

Soil site profile H220V400 – T_s = 1.3 s

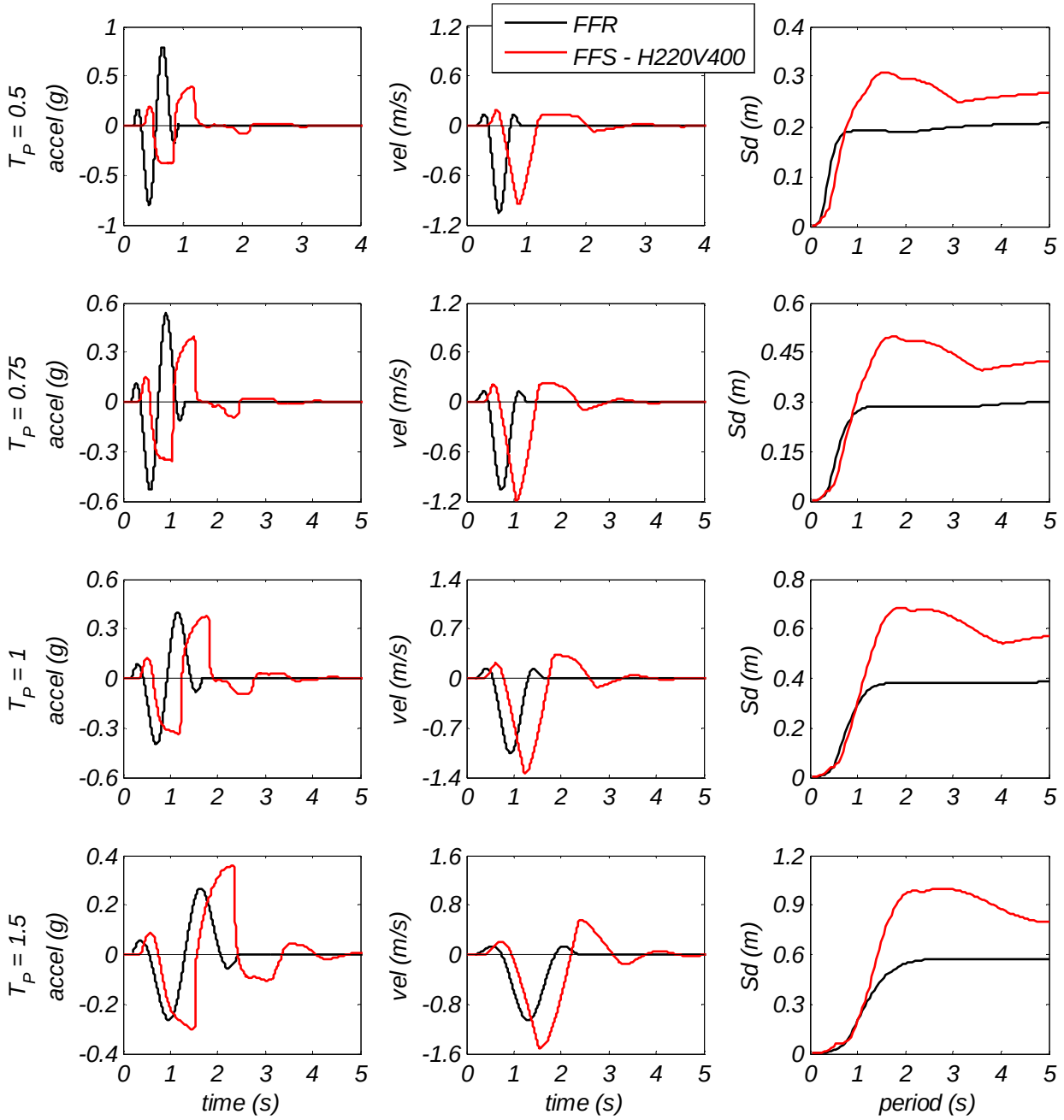

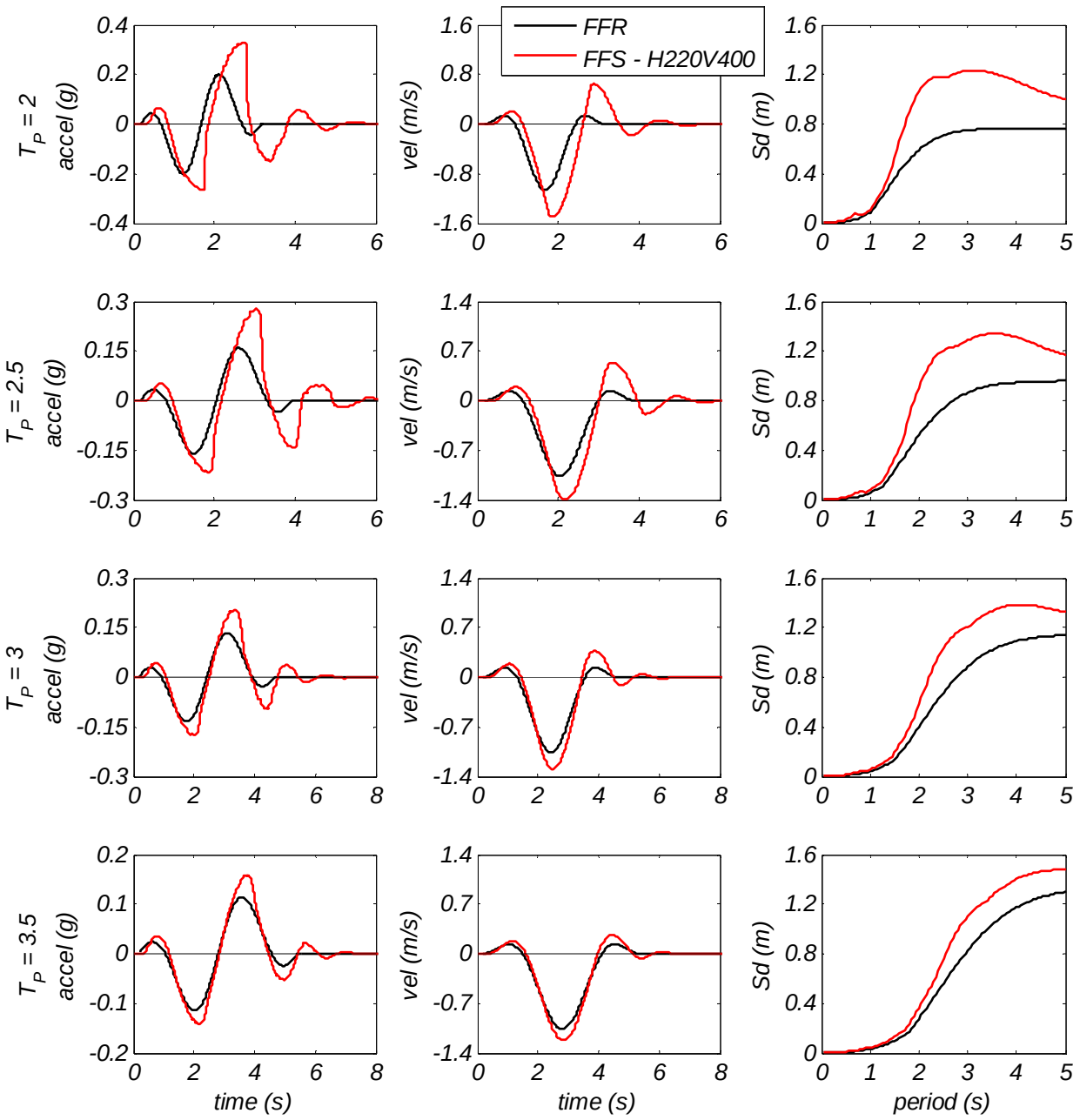
FFR
FFS - H220V400
T_P = 2
T_P = 2.5
T_P = 3
T_P = 3.5
accel (g)
vel (m/s)
Sd (m)
time (s)
period (s)

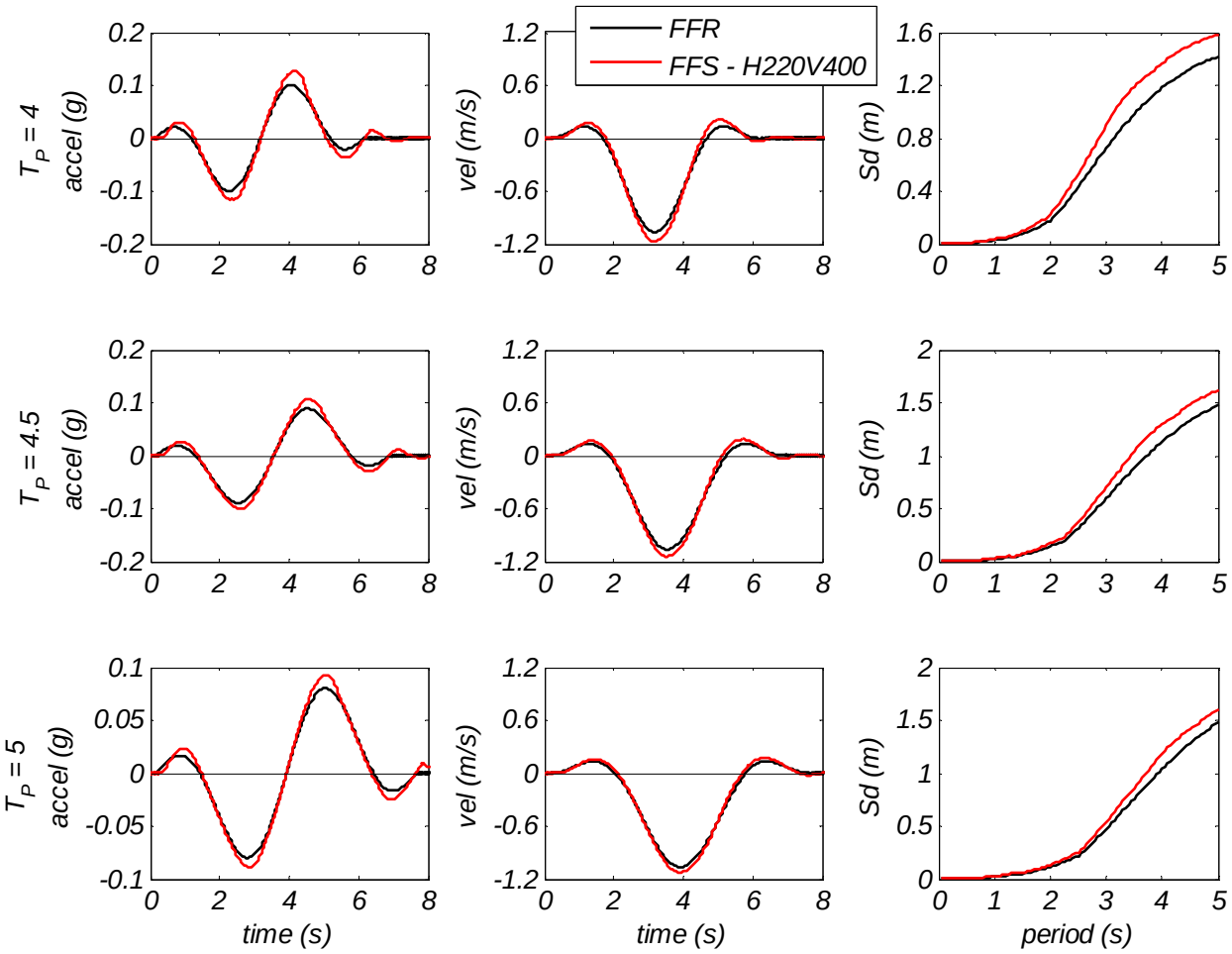
FFR
FFS - H220V400
T_P = 4
T_P = 4.5
T_P = 5
accel (g)
vel (m/s)
Sd (m)
time (s)
time (s)
period (s)

Soil site profile H220V200 – T_s = 1.6 s

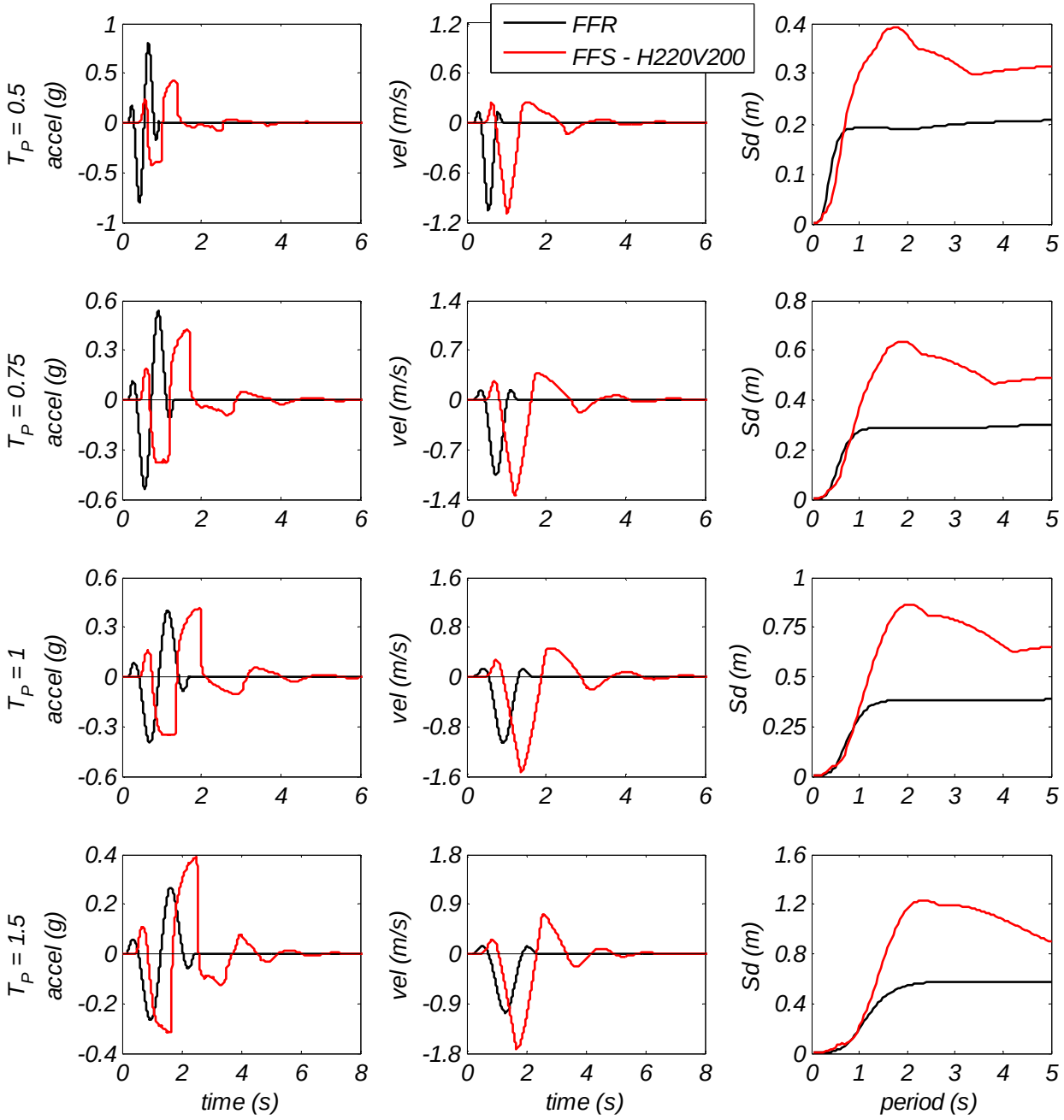

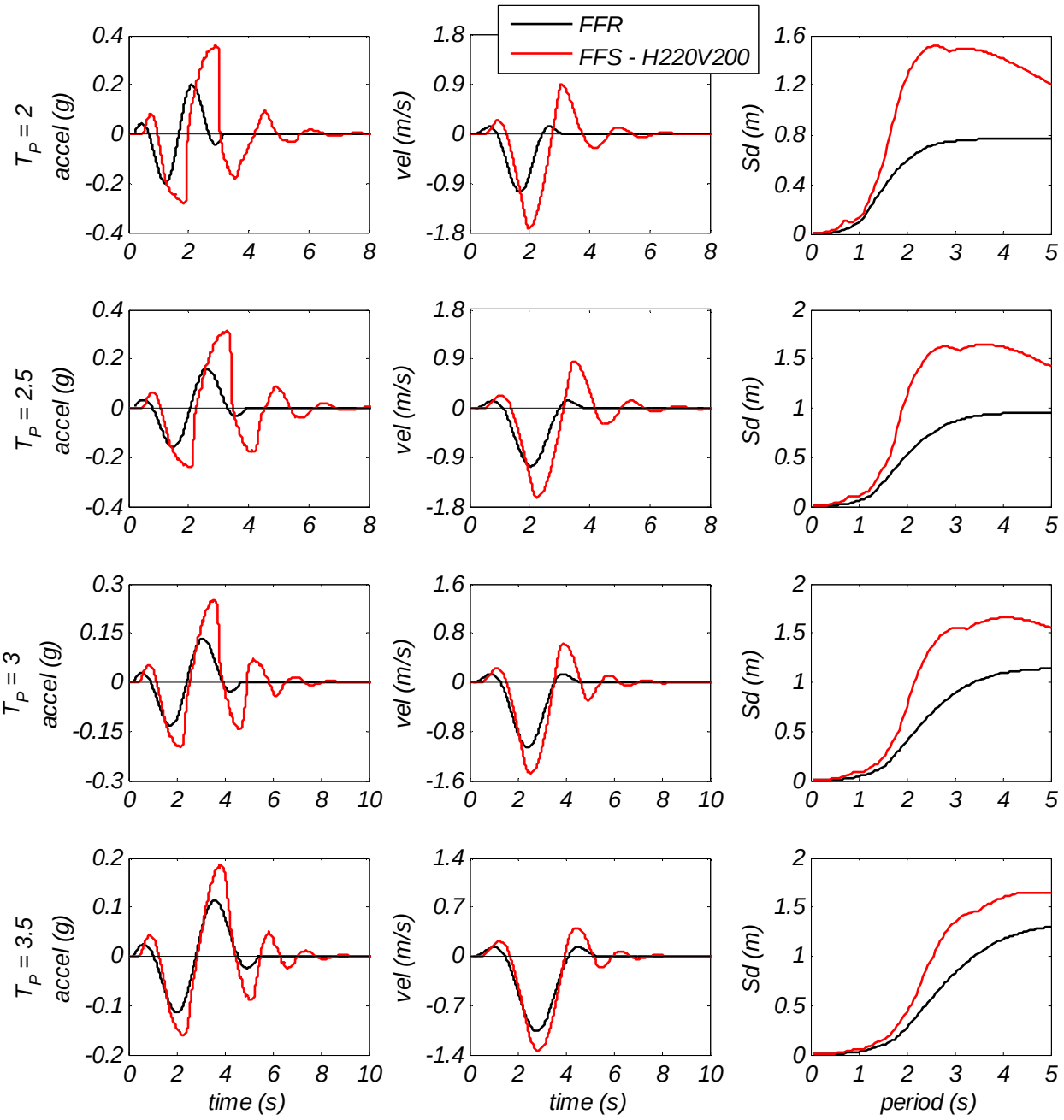
FFR
FFS - H220V200
T_P = 2
T_P = 2.5
T_P = 3
T_P = 3.5
accel (g)
vel (m/s)
Sd (m)
time (s)
period (s)

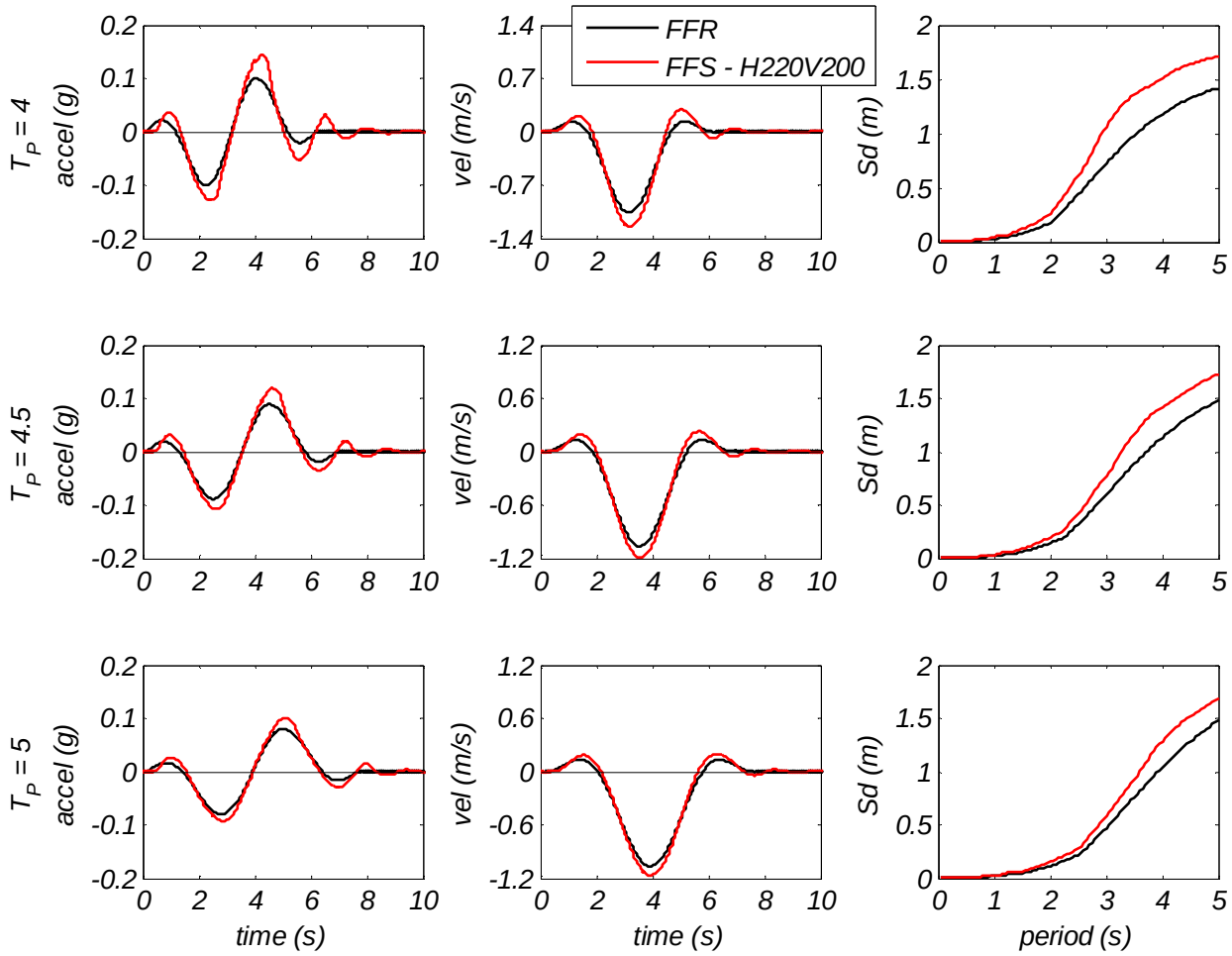
FFR
FFS - H220V200
T_P = 4
T_P = 4.5
T_P = 5
accel (g)
vel (m/s)
Sd (m)
time (s)
time (s)
period (s)